行政院國家科學委員會補助專題研究計畫 ■成果報告 □期中進度報告

計畫名稱：以掃描探針研究聚合高分子中染色分子為區及畫與臨場分析其極畫之動態行為

Local Poling of the Polar Chromophores in Copolymers and in situ Micro Characterization of the Polarization Dynamics by Scanning Probes

計畫類別：■個別型計畫　□整合型計畫
計畫編號：NSC　96－2112－M－029－005－MY3
執行期間：　2007 年 8 月 1 日至 2010 年 9 月 30 日

執行機構及系所：東海大學物理系

計畫主持人：簡世森
共同主持人：
計畫參與人員：博士生 林志遠
碩士生 江俊皇、賴冠龍、鄭承恩、陳冠霖、黃俊榮、吳易達
楊贊樺、黃千俊、張好裕
專題生 何若華、崔博婷、郭中竣、黃侶棋、張立欣

成果報告類型(依經費核定清單規定繳交)：□精簡報告　■完整報告

本計畫除繳交成果報告外，另須繳交以下出國心得報告：
■赴國外出差或研習心得報告
□赴大陸地區出差或研習心得報告
■出席國際學術會議心得報告
□國際合作研究計畫國外研究報告
處理方式：除列管計畫及下列情形者外，得立即公開查詢
□涉及專利或其他智慧財產權，□一年□二年後可公開查詢

中、英文摘要及關鍵詞 (keywords)。

含偶氮聚合高分子是一種包含 disperse red 1 (DR1) 光反應材料，近來引起多方之注意，因爲 DR1 是一獨特具極性之非線性光學染色分子。其極化強度可以透過光輔助極化之作用而產生，因爲分子有相同之排列方向。我們以掃描探針進行微區之光輔助極化，並以靜電力顯微鏡分析其極化強度。DR1 含偶氮聚合高分子之掃描探針光輔助極化由 angular hole burning 與 angular distribution(AR) 兩項反應決定其極化情形，遵守雙指數函數之行爲。其中 AR 的特徵時間與極化電壓成反比。我們發展出一個可以描述極化點之外型的公式以預測在不同電壓下，極化強度隨時間在空間之變化。

The azo copolymer film containing disperse red 1 (DR1) is a photoreactive material attracting much attention in the past few years, because DR1 is a polar, nonlinear-optical chromophore, exhibiting unique optical behaviors. The polar orientation created by local photo-assisted-poling (PAP) in the DR1-PMMA copolymer films was investigated by scanning probe microscopy. PAP was performed by a proximal biased probe and the polar orientation was semiquantitatively measured by electrostatic force microscopy (EFM). The polar orientation behaves as a bi-exponential function of the period of PAP, which is dominated by the fast angular hole burning and slow angular redistribution (AR). The characteristic time of AR decreases linearly with the poling bias. An expression has been developed to interpret the evolution of the Lorentzian-like shape of the poled spots. A poled spot with 150 nm FWHM was demonstrated.

Keywords: azo copolymer 含偶氮聚合高分子, photo-assisted poling 光輔助極化, scanning probe 掃描探針.

前言 Introduction

The copolymer film containing disperse red 1 (DR1) (Fig. 1) is a photoreactive material attracting much attention in the past few years, because DR1 is a polar, nonlinear-optical chromophore, exhibiting unique optical behaviors [1]. DR1, the push-pull derivative of azo-benzene molecules, has two isomers, *trans* and *cis* forms, which undergo the *trans* ⇔ *cis*

isomerization by optical pumping (referred to as photoisomerization). Molecular orientation anisotropy can is built up optically in the copolymers after several cycles of *trans* ⇔ *cis* photoisomerization pumped by a linearly polarized light (Fig. 2). This is so called photo-induced orientation (PIO). In the opposite effect, an anisotropic DR1 copolymer can be disordered by light, called photo-induced disorientation (PID). Therefore PIO and PID offer the opportunity to manipulate the optical properties of photoreactive copolymer films. Many studies have demonstrated potential applications of DR1 copolymers for active waveguide components [2], frequency conversion [3], index grating [4], and image storage [5, 6].

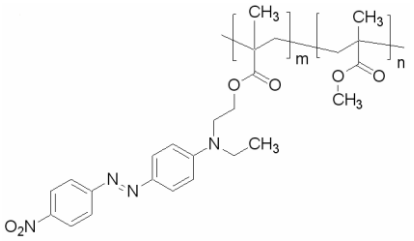

Fig. 1. Chemical structure of DR1-PMMA copolymer.

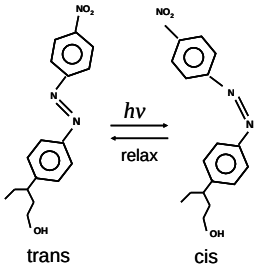

Fig. 2. trans and cis isomer forms of DR1

We employed scanning probe microscopy (SPM) to perform local photo-assisted poling (PAP) far below the glass transition temperature of DR1-PMMA copolymer thin films [7,8]. The probe acts as both an electrode to apply an electric field ($\vec{E}$) by atomic force microscopy (AFM) and a sensor to detect $\vec{P}$ *in situ* by electrostatic force microscopy (EFM) [9-11].

研究目的 **Purpose**

There is great interest in moving the applications of photoreactive materials toward the nanometer scale. However, the spatial resolution of the typical optical-based methods for poling is restricted by optical diffraction, such as nonlinear optical measurements [12,13], and attenuated total reflection [14]. To enhance the density of information storage in polymer films, some novel approaches based on scanning probe microscopy (SPM) have been demonstrated. We employed scanning probe microscopy (SPM) to perform local photo-assisted poling (PAP) far below the glass transition temperature of DR1-PMMA copolymer thin films. The probe acts as both an electrode to apply an electric field ($\vec{E}$) by atomic force microscopy (AFM) and a sensor to detect $\vec{P}$ *in situ* by electrostatic force microscopy (EFM). In this work, we studied

the kinetics of the polarization generated by probe-based PAP. The polarization behaves as a bi-exponential function of the period of PAP, and the reaction is governed by the fast angular hole burning (AHB) and the slow angular redistribution (AR). An analytical expression is introduced to interpret the evolution of the Lorentzian-like shape of the poled spot.

文獻探討

Maeda *et al*. [15] have demonstrated the polarization storage in the guest-host polymethylmethacrylate (PMMA) thin film containing disperse red one (DR1). DR1, azo-benzene molecule, is a nonlinear optical chromophore, well known for the *trans* ↔ *cis* photoisomerization excited by light [16]. The data bits were written by photo-induced orientation (PIO) which is activated by two-photon absorption (TPA) and read by a polarized confocal laser scanning microscopy in reflection mode. Maede's work inspired Zyss's group [17] to develop a new scheme towards nonlinear optical memories. The data bits were written by TPA and read by second harmonic generation (SHG) response of the nonlinear chromophores in polymer films. The spatial resolution of the polar orientation is significantly improved to the submicron scale, due to conditions in which the nonlinear processes (TPA and SHG) are confined at the vicinity of the focal point (a volume of order λ^3, where λ is the laser wavelength).

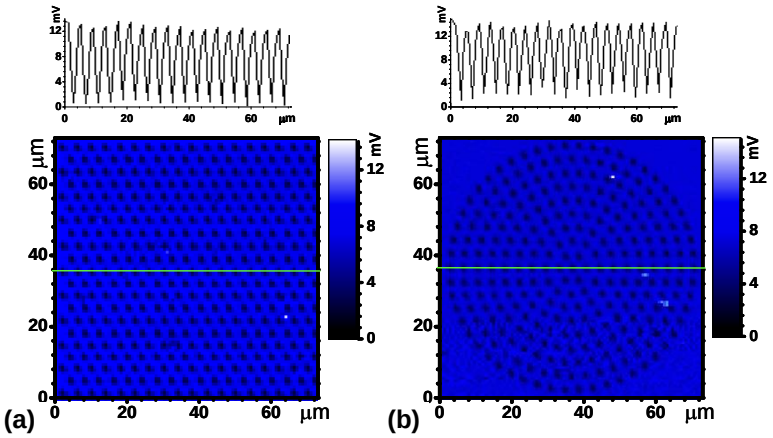

Fig. 3. The SHG mapping images in poled azo-copolymer thin films measured by the SHG mapping technique. (a) 2D hexagonal $\chi^{(2)}$ structure and (b) 2D circular $\chi^{(2)}$ structure with period = 4 μm, both fabricated by two-photon absorption DLW technique.

Dorkenoo's group [18] and Hsu's group [19] individually proposed another new approach, in which uniform orientation of DR1-PMMA copolymer film was created by corona poling and the

data bits were produced by the disorientation of the DR1 chromophores through TPA-induced photoisomerization (Fig. 3). The data can be erased by heating the copolymer film and rewritten again after repoling the film. Consequently, rewritable optical storage is accomplished.

研究方法 Approach

A commercial SPM was utilized to scan the topography and conduct local PAP (by AFM) and characterize the polarization or surface charge (by EFM) (Fig. 4). A linearly-polarized 473 nm 710 mW/cm^2 solid state laser with 3 mm diameter was used for local PAP. The illumination power was controller by an attenuator. The EFM was operated in lift mode with a lift height of 30 nm to 50 nm to map the polarization of DR1-PMMA thin films. The Si-based cantilever is metallic-coated with Ti-Pt double layers. The nominal radius of the probe apex is 20 nm. The nominal force constant and resonant frequency (f_0) of the cantilevers are 2-5 N/m and 65-70 kHz, respectively. The cantilever was stimulated at a fixed frequency near f_0. An sensing bias (–3 V or +3 V) was applied to the probe during EFM mapping.

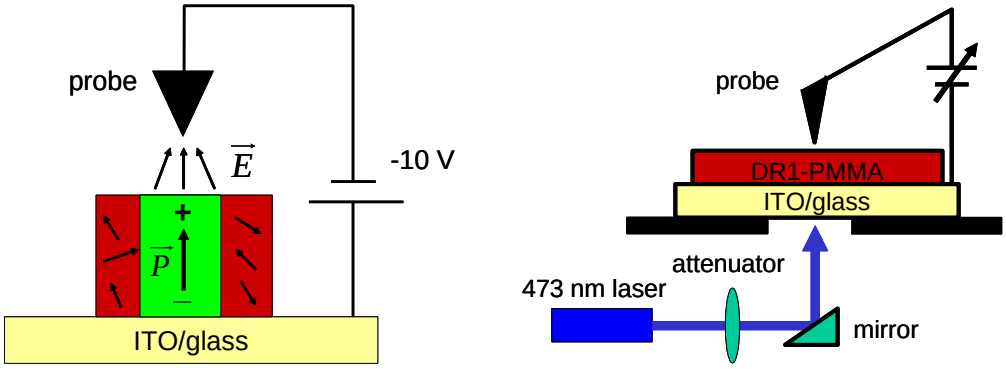

Figure 4. (a) Schematic of the relationship between the bias and electric field and polarization/bound charges associated with the local poling by a negatively-biased probe and (b) the local PAP with an illumination of a laser source from the back side

The Coulomb force between the biased probe and σ_b, given by $-\sigma_b\vec{E}$, introduces an extra force gradient to the probe, leading to a shift of resonant frequency. The phase of the cantilever (ϕ) responds sensitively to the extra force gradient and the EFM maps the phase shift ($\Delta\phi$) of the cantilever with a lock-in amplifier to observe the variation of external force over the surface. An

attractive/repulsive extra force causes a negative/positive phase shift, corresponding to a lower/higher (darker/brighter) EFM signal level. Therefore, given the imaging bias, the gray scale of the EFM images can represent both the magnitude and sign of surface charges. The determination of the sign of the surface charges is critical to judge which effect (PAP or CE) induces the charges.

結果與討論 Results and Discussion

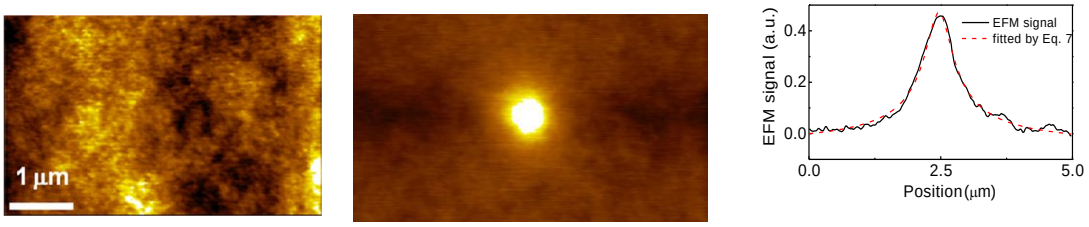

Fig. 5. (a) and (b) Topographic and EFM images of a poled spot induced by local PAP on a DR1-PMMA copolymer film. (c) The profile of the EFM image along the dashed line in (b).

The topographic and the EFM images were taken simultaneously, as shown in Fig. 4. The cross-sectional profile of the EFM image in Fig. 4(c) shows that the polarization is characterized by a Lorentzian-like shape. The peak of the induced polarization $P_p(t)$ as a function of t was studied under the illumination of various laser powers (10, 80 and 550 μW) and a fixed bias (－10 V). As shown in Fig. 6(a), $P_p(t)$ grows as a bi-exponential function of t [20], described by the following equation:

$$P_p(t) = P_0[1 - a_1 \exp(-t/\tau_1) - a_2 \exp(-t/\tau_2)], \quad (1)$$

where P_0 is the saturated polarization, τ_1 and τ_2 are the response times of the chromophores to PAP, and a_1 and a_2 are coefficients of the exponential terms.

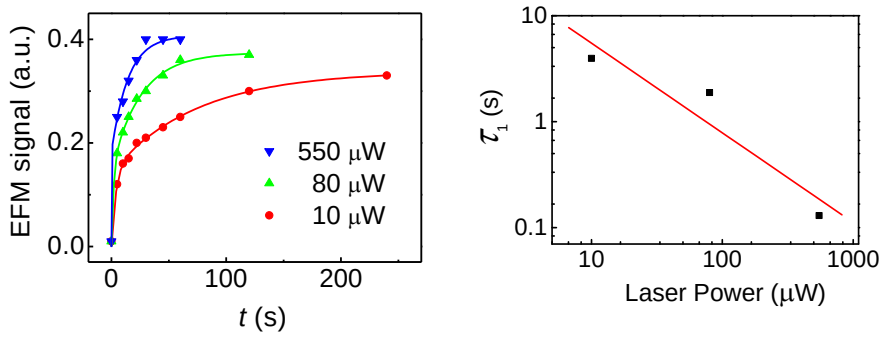

Fig. 6. (a) Peak of the polarization (P_p) *vs*. the period of local PAP (t) under various laser powers, and (b) plot of the characteristic time τ_1 as a function of laser power (P_L).

The buildup of the polar orientation is associated with two reactions; namely the fast AHB and slow AR [21,22]. AHB involves the transition of *trans* → *cis* by optical pumping, and results in the increase in the population of *cis* state. Contrarily, AR involves the orientation diffusion of the *cis* chromophores driven by the torque and the thermal agitation. Therefore, τ_i and a_i (i = 1, 2) can be regarded as the characteristic time and the weight of the reactions of AHB and AR.

According to the values of the fitted parameters, τ_1 and τ_2 behaves differently in response to the laser power, and τ_1 is a few orders of magnitude shorter than τ_2. Note that τ_1 is inversely proportional to the laser power ($\propto P_L^{-1}$) as shown in Fig. 3(b), while τ_2 is less sensitive to P_L. We consider τ_1 to be the characteristic time of the *trans* → *cis* transition (also referred to as *pumping time*), since the pumping time is proportional to $(\sigma_t \Phi_{tc} P_L)^{-1}$, with σ_t representing the cross sections for the absorption of one photon by a *trans*-chromophore, and Φ_{tc} the quantum yield of *trans* → *cis* photoisomerization [21]. Also, P_0 increases with P_L, because a high P_L gives a higher population of the rotatable *cis*-molecules.

We also analyzed $P_p(t)$ induced under various biases V (– 2 V, – 5 V and – 10 V) with a constant laser power exposure (100 μW). As illustrated in Fig. 4(a), $P_p(t)$ still obeys the bi-exponential behavior. We observed the empirical dependence of P_0 on the bias in a square-root relation, given as $P_0(V) = \alpha\sqrt{|V| - V_o}$ (= 0.07 is a constant and V_o = 0.97 V is the threshold bias). The polarization was not detectable as the bias fell below the threshold bias V_o. The threshold bias depends on the film thickness and the probe condition. Based on this relationship, Eq. (1) can be

rewritten as

$$P_p(V,t) = P_0(V)\,[1 - a_1 \exp(\frac{-t}{\tau_1}) - a_2 \exp(\frac{-t}{\tau_D^c - \beta|V|})] \tag{3}$$

$P_p(V, t)$ is an explicit function of bias, and τ_2 decreases linearly with the bias as shown in Fig. 4(b). $P_p(V, t)$ is an explicit function of bias. As we take into account the distribution of the electric field, Eq. 3 can be modified to describe the Lorentzian-like shape of P. We propose that the poling electric field under the probe is represented by $V \cdot L(\rho,\sigma)$, where $L(\rho,\sigma) = \frac{\sigma^2}{4\rho^2 + \sigma^2}$ is the Lorentzian function of radial distance ρ, and σ stands for the half width. The Lorentzian field could result from the geometry of the probe. Taking the field distribution into account, the polarization can be expressed as

$$P(\rho,V,t) = P_0(V,\rho)\,[1 - a_1 \exp(\frac{-t}{\tau_1}) - a_2 \exp(\frac{-t}{\tau_D^c - \beta|V| \cdot L(\rho,\sigma)})], \tag{4}$$

where $P_0(V,\rho) = \alpha\sqrt{|V| \cdot L(\rho,\sigma) - V_o}$ the saturated polarization involving the field distribution. As $|V| \cdot L(\rho,\sigma) < V_o$, the effect of PAP is ignored.

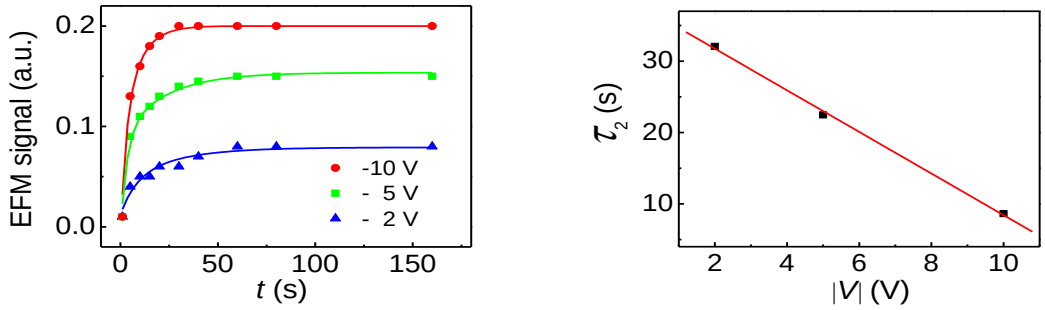

Fig. 7. (a) P_p *vs.* t under various poling biases, and (b) plot of the characteristic time τ_2 as the function of the bias.

According to these analyses, the optimum period of PAP to generate minimum poled spots on the film was obtained. A poled spot of 150 nm FWHM was made by a fresh probe with V = – 3 V and t = 30 s, as shown in Fig. 8. Such a size is well below those produced by other optical-induced orientation on photoreactive films.

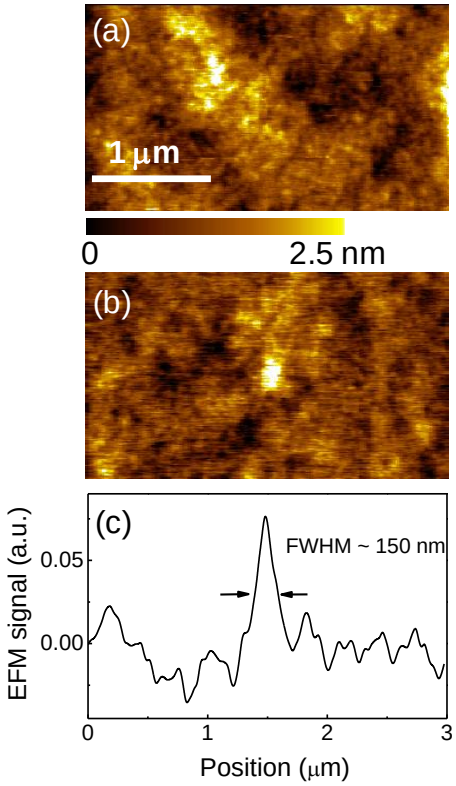

Fig. 8. (a) and (b) Topographic and EFM images of a poled spot with 150 nm.FWHM, and (c) the profile of EFM signal along the center of the poled spot in (b).

參考文獻

1. Sekkat Z and Knoll W 2002 *Photoreactive Organic Thin Films*, ed (San Diego, CA: Academic), and references therein.

2. Donval A, Toussaere E, Hierle R and Zyss J 2000 J. Appl. Phys. **87** 3258.

3. Martin G, Ducci S, Josse D and Zyss J 2003 Appl. Phys. Lett. **83** 1086.

4. Zhang W, Bian S, Kim S I and Kuzyk M G 2002 Opt. Lett. **27** 1105.
5. Sekkat Z, Wood J, Knoll W, Volksen W, Miller R D and Knoesen A 1997 J. Opt. Soc. Am. **B14** 829.
6. Matsuoka N, Kitaoka K, Si J, Fujita K and Hirao K 2000 Opt. Commun. **185** 467.
7. Sekkat Z, Kang C-S, Aust E F, Wegner G and Knoll W 1995 Chem. Mater. **7** 142.
8. Blanchard P M and Mitchell G R 1993 Appl. Phys. Lett. **63** 2038.
9. Terris B D, Stern J E, Rugar D and Mamin H J 1989 Phys. Rev. Lett. **63** 2669.
10. Dianoux R, Martins F, Marchi F, Alandi C, Comin F and Chevrier J 2003 Phys. Rev. B **68** 045403.
11. Xu Q and Hsu J W P 1999 J. Appl. Phys. **85** 2465.
12. Lin J H, Lai N D, Chiu C H, Lin C-Y, Rieger G W, Young J F, Chien F S-S, and Hsu C C 2008 *Opt. Express* **16** 7832.
13. Sekkat Z, Kang C-S, Aust E F, Wegner G, and Knoll W 1995 *Chem. Mater.* **7** 142
14. Ishitobi H, Tanabe M, Sekkat Z and Kawata S 2007 *Appl. Phys. Lett.* **91** 091911
15. Maeda M, Ishitobi H, Sekkat Z, and Kawata S 2004 *Appl. Phys. Lett.* **85** 351
16. Sekkat Z and Knoll W 2002 *Photoreactive Organic Thin Films*, ed (San Diego, CA: Academic)
17. Martin G, Ducci S, Josse D, and Zyss J 2003 *Appl. Phys. Lett.* **83** 1086
18. Gindre D, Boeglin A, Fort A, Mager L, and Dorkenoo K D 2006 *Opt. Express* **14**, 9896
19. Lin J H, Lai N D, Chiu C H, Lin C-Y, Rieger G W, Young J F, Chien F S-S, and Hsu C C 2008 *Opt. Express* **16** 7832

20. Dumont M, Sekkat Z, Loucif-Saibi R, Nakatani K, and Delaire J A 1993 *Nonlin. Opt.* 5 395

21. Sekkat Z, and Knoll W 1995 *J. Opt. Soc. Am.* B **12** 1855

22. Hsu C-C, Lin J-H, Huang T-H and Harada K 2003 Appl. Phys. Lett. **82** 2440

Polar orientation induced by local photo-assisted poling in azo copolymer films

F. S.-S. Chien,[1,*] C. Y. Lin,[2,1] C. R. Huang,[1] C. S. Chang,[2] and C. C. Hsu[3]

[1]*Department of Physics, Tunghai University, Taichung, Taiwan*
[2]*Department of Photonics and Institute of Electro-Optical Engineering, National Chiao Tung University, Hsinchu 300, Taiwan*
[3]*Department of Physics, National Chung-Cheng University, Chiayi, Taiwan*
[*]*Corresponding author: fsschien@thu.edu.tw*

Received October 5, 2009; revised January 27, 2010; accepted February 8, 2010; posted February 16, 2010 (Doc. ID 118182); published March 31, 2010

Polar orientation created by local photo-assisted poling (PAP) in copolymer films containing disperse red 1 was investigated by scanning probe microscopy. PAP was performed by a proximal biased probe, and the polar orientation was semiquantitatively measured by electrostatic force microscopy. The polar orientation behaves as a biexponential function of the period of PAP, which is dominated by fast angular hole burning and slow angular redistribution (AR). The characteristic time of AR decreases linearly with the poling bias. An expression has been developed to interpret the evolution of the Lorentzian-like shape of the poled spots. A poled spot with 150 nm FWHM was demonstrated. © 2010 Optical Society of America

OCIS codes: 160.5320, 160.5470, 180.5810, 210.1635.

1. INTRODUCTION

Optical engineering of photoreactive polymers provides an efficient and convenient approach to generate nonlinear configuration for information storage [1,2] and second-harmonic generation (SHG) [3]. Maeda *et al.* [4] have demonstrated polarization storage in the guest-host polymethylmethacrylate (PMMA) thin film containing disperse red 1 (DR1). The DR1, azo-benzene molecule is a nonlinear optical chromophore that is well known for the *trans*↔*cis* photoisomerization excited by light [5]. The data bits were written by photoinduced orientation (PIO), which is activated by two-photon absorption (TPA) and read by confocal laser scanning microscopy in reflection mode.

Zyss's group [6] developed a new scheme for nonlinear optical memories. The data bits were written by all-optical poling (AOP) and read by the SHG response of the nonlinear chromophores in polymer films. The spatial resolution of the polar orientation is significantly improved to the submicron scale, due to conditions in which the nonlinear processes (AOP and SHG) are confined in the vicinity of the focal point (a volume of order λ^3, where λ is the laser wavelength). Dorkenoo's group [7] and Hsu's group [8] separately proposed another new approach, in which uniform orientation of a DR1-PMMA copolymer film was created by corona poling and the data bits were produced by the disorientation of the DR1 chromophores through TPA-induced photoisomerization. The data can be erased by heating the copolymer film and rewritten again after repoling the film. Consequently, rewritable optical storage is accomplished.

However, the spatial resolution of the typical optical-based methods, such as nonlinear optical measurements [7,8] and attenuated total reflection [9], is restricted by optical diffraction. To enhance the density of information storage in polymer films, some novel approaches based on scanning probe microscopy (SPM) have been demonstrated. For instance, protrusions with a diameter of 50 nm were produced by metal-probe-enhanced near-field illumination [10]. Also, submicron-scale polar orientation in azo polymer films was generated by probe-induced local photo-assisted poling (PAP) [11] in which a biased proximal probe provides an intense electric field to the azo polymer films under illumination. The polarization ($\vec{P}$) was analyzed *in-situ* by electrostatic force microscopy (EFM) [12], which detects the Coulomb force $F_C = -\sigma_b \cdot \vec{E}$ acting on the probe, where σ_b ($=\vec{P}\cdot\hat{n}$, $\hat{n}$: the surface normal unit vector) stands for the surface bound charges and $\vec{E}$ the electric field. Not only does it give a higher resolution than other optical detection methods, EFM can also investigate without disturbance to the orientation. In this work, we studied the kinetics of the polarization generated by probe-based PAP. The polarization behaves as a biexponential function of the period of PAP, and the reaction is governed by the fast angular hole burning (AHB) and the slow angular redistribution (AR). An analytical expression is introduced to interpret the evolution of the Lorentzian-like shape of the poled spot.

2. EXPERIMENT

DR1-PMMA copolymer was dissolved in chloroform, filtered with a 250 nm filter, and spin-coated on a cleaned conducting indium tin oxide (ITO) glass plate. The ITO glass served as the bottom electrode. The film was then subjected to post-baking at 80 °C for 1 hour to form a film with a thickness of about 0.1 μm. The film exhibited an absorption band ranging from 400 nm to 600 nm, with an absorption peak at 470 nm. A SPM was utilized to map

the topography, perform local PAP, and analyze the polarization of the film. The probe was metallic-coated and had a nominal force constant of 2 N/m and resonant frequency (f_0) of 75 kHz. EFM mapping was accomplished by a double-path scheme. To observe the variation of polarization quantitatively over the surface, the phase shift ($\Delta\phi$) of the oscillating cantilevers was measured during the second path while the probe was biased at +3 V and lifted by 30 nm.

For implementation of local PAP, a poling bias (V) was applied to the probe and a linearly polarized diode-pumped solid-state laser was used to stimulate the *trans*⇔*cis* photoisomerization, so that the *cis*-chromophores are free to be rotated at room temperature by the torque ($\vec{\mu}_c \times \vec{E}$, μ_c: dipole moment of *cis*-chromophores,). The wavelength and the beam diameter of the laser were 473 nm and 3 mm, respectively. The laser was not focused, so we assumed the laser light is a plane wave with a horizontal polarization (perpendicular to the applied dc electric field). This configuration makes PAP more efficient. To avoid contact electrification (charge transfer) between the probe and the copolymer, the SPM was operated in tapping mode to reduce the period of physical contact during poling [11].

3. RESULTS AND DISCUSSION

A. Semiquantitative Measurement of EFM

The cantilever was stimulated with a fixed frequency near f_0. The additional force F_C associated with the polar orientation of the film introduces shifts in the resonance frequency (Δf_0) and phase ($\Delta\phi$). Within a small shift limit, the relationships $\Delta f_0 \propto \partial F_C/\partial z \propto P \cdot \partial E/\partial z$ are true [13]. Near f_0, $\Delta\phi$ responds almost linearly to the shift of resonance frequency ($\Delta\phi \propto \Delta f_0$), and the phase shift is proportional to the polarization ($\Delta\phi \propto P$) under a fixed applied E field, because of the high quality factor (>300) of the cantilever.

To validate the semiquantitative measurement of EFM, an external dc bias was applied to the probe to mimic the effect of F_C and to verify the relation $\Delta\phi \propto \partial F_C/\partial z$. Since the dc bias induces a capacitive force ($F_B = -\frac{1}{2}\partial C/\partial z V^2$), $\Delta\phi$ should obey the relation $\Delta\phi \propto -\frac{1}{2}\partial^2 C/\partial z^2 V^2$. As shown in Fig. 1, $\Delta\phi$ demonstrates a quadratic function of V, and thus assures the capability of EFM for semiquantitative measurement of polarization.

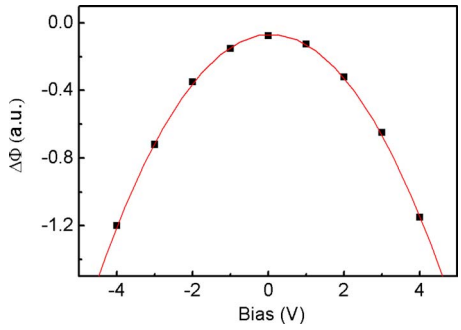

Fig. 1. (Color online) Phase shift ($\Delta\phi$) of an oscillating cantilever as a function of the bias.

B. Polarization *vs.* Laser Power

The film was subjected to a bias of +10 V and a laser power (P_L) of 500 μW for 360 s to achieve local PAP, while the oscillating probe was held still over the surface. The period of PAP (t) was equivalent to the time during which both the bias and laser were applied. The topographic and the EFM images were taken simultaneously, as shown in Figs. 2(a) and 2(b). The cross-sectional profile of the EFM image in Fig. 2(c) shows that the polarization is characterized by a Lorentzian-like shape. No plasmonic effect was produced to amplify the light at the probe apex, because there is no component with vertical laser polarization. Therefore, in Fig. 2(a), no remarkable change appears to the topography due to mass transport after PAP. Analytical expressions for nonlocal PAP-induced polarization based on a phenomenological theory have been presented [13]. Based on the theory, the polarization is associated with the molecular orientation as $\vec{P}(t) = N\mu_t 3T_1(t)/5\hat{z}$, where N is the molecular density of DR1 and $T_1(t)$ the first-order coefficient of the non-normalized Legendre expansion for the molecular angular distribution [14,15]. We assume that the contribution of *cis*-chromophores to the polarization is negligible. The peak of the induced polarization $P_p(t)$ as a function of t was studied under the illumination of various laser powers (10, 80, and 550 μW) and a fixed bias (−10 V). As shown in Fig. 3(a), $P_p(t)$ grows as a biexponential function of t [16], described by the following equation:

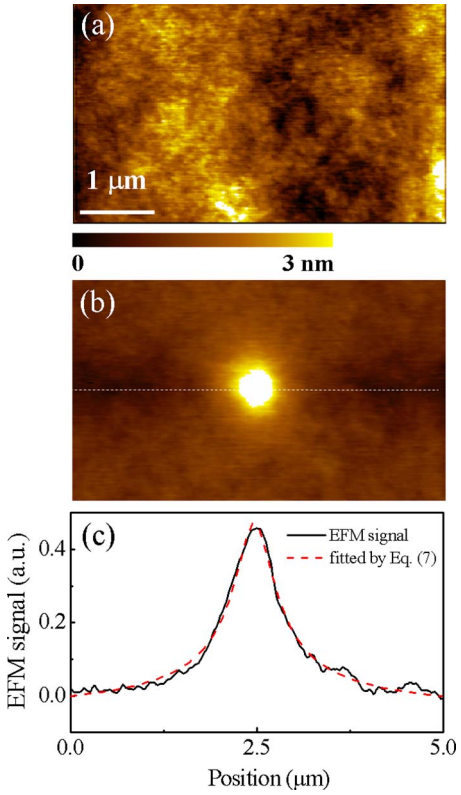

Fig. 2. (Color online) (a) and (b) Topographic and EFM images of a poled spot induced by local PAP on a DR1-PMMA copolymer film. (c) The profile of the EFM signal along the dashed line in (b).

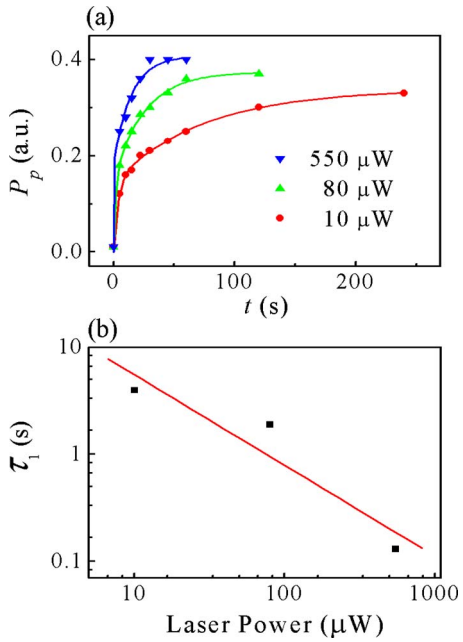

Fig. 3. (Color online) (a) Peak of the polarization (P_p) versus the period of local PAP (t) under various laser powers. (b) Plot of the characteristic time τ_1 as a function of laser power (P_L).

$$P_p(t) = P_0[1 - a_1 \exp(-t/\tau_1) - a_2 \exp(-t/\tau_2)], \qquad (1)$$

where P_0 is the saturated polarization, τ_1 and τ_2 are the response times of the chromophores to PAP, and a_1 and a_2 are coefficients of the exponential terms. The parameters were fitted according to Eq. (1), with the resulting values listed in Table 1. Note that P_0 is a function of the bias and laser power, and $a_1+a_2 \cong 1$.

The buildup of the polar orientation is associated with two reactions; namely, the fast AHB and slow AR [14,16]. AHB involves the *trans*→*cis* transition by optical pumping, and it results in an increase in the population of *cis* state. Contrarily, AR involves the orientation diffusion of the *cis* chromophores driven by the torque and the thermal agitation. Therefore, τ_i and a_i ($i=1,2$) can be regarded as the characteristic time and the weight of the reactions of AHB and AR. It is believed that, in the presence of an intense electric field, most molecules preserve the memory of orientation during the back-isomerization.

According to the values of the fitted parameters (Table 1), τ_1 and τ_2 behave differently in response to the laser power, and τ_1 is a few orders of magnitude shorter than τ_2. Note that τ_1 is inversely proportional to the laser power ($\propto P_L^{-1}$) as shown in Fig. 3(b), while τ_2 is less sensitive to P_L. We consider τ_1 to be the characteristic time of the *trans*→*cis* transition (also referred to as *pumping time*), since the pumping time is proportional to $(\sigma_t \Phi_{tc} P_L)^{-1}$, with σ_t representing the cross section for the absorption of one photon by a *trans*-chromophore, and Φ_{tc} the quantum yield of *trans*→*cis* photoisomerization [13]. Also, P_0 increases with P_L, because a high P_L gives a higher population of the rotatable *cis*-molecules.

Table 1. Values of the Fitted Parameters in Eq. (1) under Various Laser Powers

I (μW)	τ_1 (s)	τ_2 (s)	a_1	a_2	P_0
10	4.0	75	0.38	0.56	0.34
80	1.9	25	0.38	0.59	0.37
550	0.13	16	0.39	0.58	0.43

C. Polarization *vs.* Bias

We also analyzed $P_p(t)$ induced under various biases V (−2 V, −5 V, and −10 V) with a constant laser power exposure (100 μW). As illustrated in Fig. 4(a), $P_p(t)$ still obeys the biexponential behavior, and the values of the fitted parameters (P_0, τ_1, τ_2, a_1, and a_2) are listed in Table 2. τ_1 essentially remains constant (~2.9 s), having no apparent correlation with the bias because the *trans*→*cis* transition does not react to the bias. However, τ_2 decreases linearly with the bias as shown in Fig. 4(b). Therefore, we consider τ_2 as the angular diffusion time of AR under the poling electric field. Apparently τ_2 decreases with $|V|$ and thus is modified as

$$\tau_2 = \tau_D^c - \beta|V|, \qquad (2)$$

where τ_D^c=37.5 s is the onset of angular diffusion time for the *cis* state due to thermal effect, and β=2.9 is a proportionality coefficient that depends on the condition of the probe. The torque ($\vec{\mu}_c \times \vec{E}$) accelerates the angular diffusion of the chromophores to a specific direction, so the angular diffusion time should be associated with the bias.

According to the theory in [12], the angular diffusion is attributed to the thermal agitation of Brownian motion. The angular diffusion time is expressed as $\tau_D^c \propto \xi/kT$, where ξ, k, and T denote the viscosity of the *cis*-chromophores, the Boltzmann constant, and the absolute temperature, respectively. The electric field E is not directly involved with τ_D^c but appears as a prefactor in the expression of $T_1(t)$ (Eqs. 22 and 24 in Ref. [14]). The polar orientation increases with the strength of poling dc E

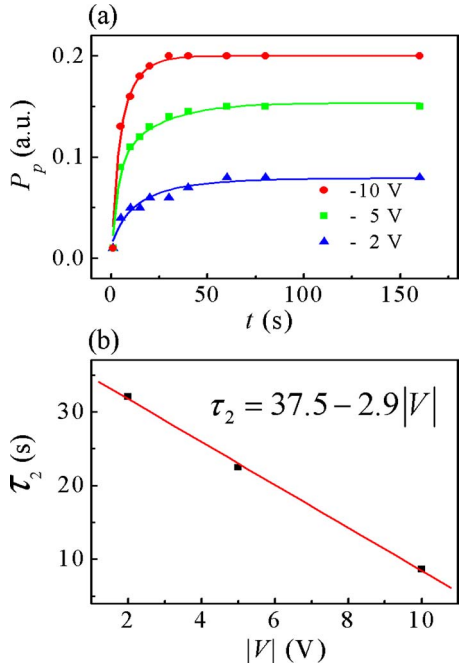

Fig. 4. (Color online) (a) P_p versus t under various poling biases. (b) Plot of the characteristic time τ_2 as a function of the bias.

Table 2. Values of the Fitted Parameters in Eq. (1) under Various Biases

Bias (V)	τ_1 (s)	τ_2 (s)	a_1	a_2	P_0
−2	2.9	32	0.56	0.50	0.08
−5	3.3	22	0.41	0.62	0.15
−10	2.8	8	0.50	0.50	0.20

field. Effectively, the angular diffusion time decreases with E, which is consistent with our observation.

It has been predicted that P_0 increases with the poling field [14]. As illustrated in Fig. 5, we observed the empirical dependence of P_0 on the bias in a square-root relation, given as $P_0(V)=\alpha\sqrt{|V|-V_0}$ ($\alpha=0.07$ is a constant and $V_o=0.97$ V is the threshold bias). The polarization was not detectable as the bias fell below the threshold bias V_o. The threshold bias depends on the film thickness and the probe condition. Based on this relationship, Eq. (1) can be rewritten as

$$P_p(V,t)=P_0(V)\left[1-a_1\exp\left(\frac{-t}{\tau_1}\right)-a_2\exp\left(\frac{-t}{\tau_D^c-\beta|V|}\right)\right]. \tag{3}$$

$P_p(V,t)$ is an explicit function of bias. As we take into account the distribution of the electric field, Eq. (3) can be modified to describe the Lorentzian-like shape of P. We propose that the poling electric field under the probe is represented by $V\cdot L(\rho,\sigma)$, where $L(\rho,\sigma)=\sigma^2/4\rho^2+\sigma^2$ is the Lorentzian function of radial distance ρ, and σ stands for the half width. The Lorentzian field could result from the geometry of the probe. Taking the field distribution into account, the polarization can be expressed as

$$P(\rho,V,t)=P_0(V,\rho)\left[1-a_1\exp\left(\frac{-t}{\tau_1}\right)-a_2\exp\left(\frac{-t}{\tau_D^c-\beta|V|\cdot L(\rho,\sigma)}\right)\right], \tag{4}$$

where $P_0(V,\rho)=\alpha\sqrt{|V|\cdot L(\rho,\sigma)-V_0}$ is the saturated polarization involving the field distribution. As $|V|\cdot L(\rho,\sigma)<V_o$, the effect of PAP is ignored. According to Eq. (4), we plotted the profile of PAP polarization with t, shown in Fig. 6, to simulate the evolution of the polarization with

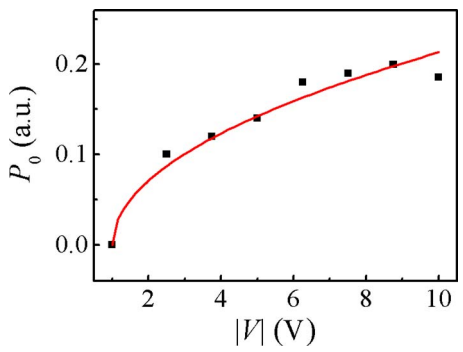

Fig. 5. (Color online) Plot of the saturated polarization (P_0) versus the poling bias.

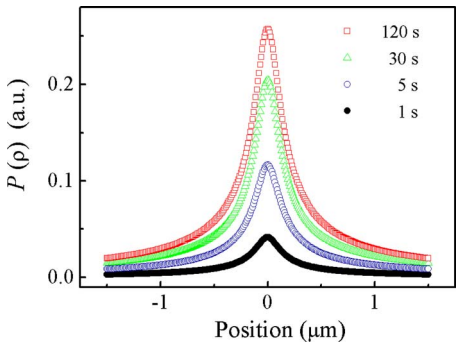

Fig. 6. (Color online) Evolution of the polarization profile $P(\rho)$ simulated by Eq. (4).

the following parameters: $V=-3$ V, $\tau_1=2.35$ s, $\tau_D^c=37.5$ s, $a_1=0.4$, $a_2=0.6$, $\sigma=235$ nm, $\alpha=0.15$, and $\beta=2.9$.

D. Evolution of the FWHM of Poled Spots

Because τ_2 varies with ρ, the polarization profile of the poled spots grows nonconformally. Therefore, the full width at half-maximum (FWHM) varies with t. Figure 7 shows the dependence of $P_p(t)$ and FWHM on t under a bias of −3 V and a laser power of 150 μW. It is evident that FWHM changes with t abnormally. Initially, FWHM decreases rapidly with t and reaches its minimum (370 nm) at ~30 s; then it increases slowly with t to reach the saturated point. The FWHM of the numerically derived profiles in Fig. 6 follows the same trends as shown in Fig. 7. Such a phenomenon can be understood through Eq. (4). In the beginning ($t\ll\tau_2$), Eq. (4) is approximated as

$$P(\rho,V,t)=P_0(V,\rho)\left[a_1\left(1-\exp\left(\frac{-t}{\tau_1}\right)\right)\right]. \tag{5}$$

During this period, the polarization is dominated by the fast AHB, and the FWHM is mainly determined by the width of P_0 (V,ρ). As t increases, AR begins to influence the growth of polarization. When $t\gg\tau_1$, Eq. (4) is approximated as

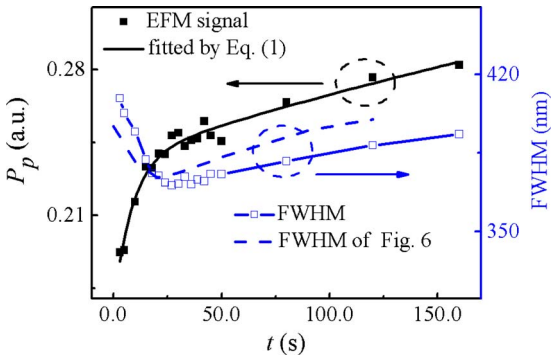

Fig. 7. (Color online) Evolution of P_p and FWHM of a poled spot created by −3 V bias and 150 μW laser, along with the FWHM predicted by Eq. (4). The FWHM of $P(\rho)$ in Fig. 6 is also shown (dashed curve).

$$P(\rho,V,t) = P_0(V,\rho)\left[1 - a_2 \exp\left(\frac{-t}{\tau_D^c - \beta|V| \cdot L(\rho,\sigma)}\right)\right]. \quad (6)$$

Under this circumstance, τ_2 increases with ρ, so AR presents a ρ-dependent enhancement to the growth of polarization. The enhancement of the AR-related factor decreases with ρ, i.e., $P(\rho=0,V,t)$ grows faster than the outer area. When $P(\rho=0,V,t)$ approaches its saturated point, the FWHM of $P(\rho V,t)$ reaches its minimum.

Afterward, the outer area around $\rho=0$ gradually reaches the saturated point, so FWMH increases with t until the poling effect terminates. Therefore when $t \gg \tau_2$, Eq. (6) becomes

$$P(\rho,V,t \gg \tau_2) \cong P_0(V,\rho), \quad (7)$$

, which suggests that the saturated FWHM should be close to the initial FWHM. The profile of the saturated polarization shown in Fig. 2 is well fitted by Eq. (7) ($\alpha=0.72$ and $\sigma=500$ nm) to demonstrate its validity.

There is a little discrepancy between the experimental and theoretical FWHMs in Fig. 7. We regard the major cause of the discrepancy to be the fact that the effect of the "vector" electric field was overestimated by the "scalar" Lorentzian potential field.

According to these analyses, the optimum period of PAP for generating minimum poled spots on the film was obtained. A poled spot of 150 nm FWHM was made by a fresh probe with $V=-3$ V and $t=30$ s, as shown in Fig. 8.

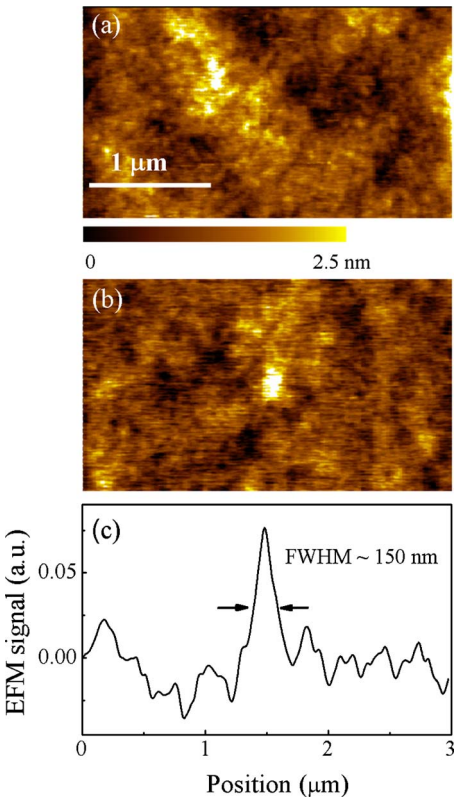

Fig. 8. (Color online) (a) and (b) Topographic and EFM images of a poled spot. (c) Profile of EFM signal along the center of the spot in (b) to show its FWHM (150 nm).

Such a size is well below those produced by other optical-induced orientation methods on photoreactive films.

The efficiency of the induced polar orientation is a major concern to the applications of photoreactive polymers. PAP is more efficient than the methods in which only optical photoinduced orientation is involved. Normally, τ_2 is much longer than τ_1, so the slow AR is the limiting process for inducing orientation. The efficiency can be improved as τ_2 is reduced by the E field in PAP; an estimate by Eq. (2) indicates that τ_2 can be reduced by 50% with a 20 V bias. In addition, the carrier-to-noise ratio is also improved by PAP, for P_0 is enhanced with the E field. It is worth noting that P_0 cannot be enhanced simply by the increase of the intensity of light [17], because the rates of *cis*→*trans* transition and the thermal angular diffusion increase as well. However, we did not observe any decrease of P_0, even as the laser power increased by two orders of magnitude. This result could be attributed to the decrease in τ_2 and the higher memory of the molecular alignment of *cis*→*trans* transition. Therefore, local PAP with scanning probes is an efficient method for the creation of polar orientation.

4. CONCLUSION

The polar orientation of local PAP in DR1-PMMA copolymer films was induced by scanning probes and investigated by EFM. The polar orientation obeys a biexponential function of the period of PAP. The kinetics is dominated by the characteristic times of AHB and AR. The poling field can effectively reduce the characteristic time of AR. An analytical expression depicting the Lorentzian-like shape of the poled spots was derived, and the evolutions of the polarization as well as the FWHM of the spots were interpreted. Local PAP is a more efficient approach than all-optical methods to generate subdiffraction-limit polar orientation. A poled spot of 150 nm FWHM was produced.

ACKNOWLEDGMENTS

The authors gratefully acknowledge the support of the National Science Council of Taiwan under grant NSC 96-2112-M-029-005-MY3.

REFERENCES

1. Z. Sekkat, J. Wood, W. Knoll, W. Volksen, R. D. Miller, and A. Knoesen, "Light-induced orientation in azo-polyimide polymers 325 °C below the glass transition temperature," J. Opt. Soc. Am. B **14**, 829–833 (1997).
2. N. Matsuoka, K. Kitaoka, J. Si, K. Fujita, and K. Hirao, "Second-order nonlinearity and optical image storage in phenyl-silica hybrid films doped with azo-dye chromophore using optical poling technique," Opt. Commun. **185**, 467–472 (2000).
3. G. Martin, S. Ducci, R. Hierle, D. Josse, and J. Zyss, "Quasi-phase matched second-harmonic generation from periodic optical randomization of poled polymer channel waveguides," Appl. Phys. Lett. **83**, 1086–1088 (2003).
4. M. Maeda, H. Ishitobi, Z. Sekkat, and S. Kawata, "Polarization storage by nonlinear orientational hole burning in azo dye-containing polymer films," Appl. Phys. Lett. **85**, 351–353 (2004).
5. Z. Sekkat, "Photo-orientation by photoisomerization," in

Photoreactive Organic Thin Films, Z. Sekkat and W. Knoll eds. (Academic, Elsevier Science, 2002), Chap. 3.
6. S. Bidault, J. Gouya, S. Brasselet, and J. Zyss, "Encoding multipolar polarization patterns by optical poling in polymers: towards nonlinear optical memories," Opt. Express **83**, 505–509 (2005).
7. D. Gindre, A. Boeglin, A. Fort, L. Mager, and K. D. Dorkenoo, "Rewritable optical data storage in azobenzene copolymers," Opt. Express **14**, 9896–9900 (2006).
8. J. H. Lin, N. D. Lai, C. H. Chiu, C.-Y. Lin, G. W. Rieger, J. F. Young, F. S.-S. Chien, and C. C. Hsu, "Fabrication of spatial modulated second order nonlinear structures and quasi-phase matched second harmonic generation in a poled azo-copolymer planar waveguide," Opt. Express **16**, 7832–7841 (2008).
9. Z. Sekkat, C.-S. Kang, E. F. Aust, G. Wegner, and W. Knoll, "Room-temperature photoinduced poling and thermal poling of a rigid main-chain polymer with polar azo dyes in the side chain," Chem. Mater. **7**, 142–147 (1995).
10. H. Ishitobi, M. Tanabe, Z. Sekkat, and S. Kawata, "Nano-movement of azo polymers induced by metal tip enhanced near-field irradiation," Appl. Phys. Lett. **91**, 091911 (2007).
11. F. S.-S. Chien, C. Y. Lin, and C. C. Hsu, "Local photo-assisted poling azo copolymer films by scanning probe microscopy," J. Phys. D: Appl. Phys. **41**, 235502 (2008).
12. D. Sarid, *Scanning Force Microscope: with applications to electric, magnetic, and atomic forces* (Oxford Univ. Press, 1991).
13. M. J. Gordon and T. Baron, "Amplitude-mode electrostatic force microscopy in UHV: quantification of nanocrystal charge storage," Phys. Rev. B **72**, 165420 (2005).
14. Z. Sekkat and W. Knoll, "Creation of second-order nonlinear optical effects by photoisomerization of polar azo dyes in polymeric films: theoretical study of steady-state and transient properties," J. Opt. Soc. Am. B **12**, 1855–1867 (1995).
15. G. Xu, X. Liu, J. Si, P. Ye, Z. Li, and Y. Shen, "Modified theory of photoinduced molecular polar alignment in azo polymers," Opt. Lett. **25**, 329–331 (2000).
16. C.-C. Hsu, J.-H. Lin, T.-H. Huang, and K. Harada, "Temperature-dependent photoinduced third-harmonic-generation variation in azo-homopolymer and azo-doped polymer thin films," Appl. Phys. Lett. **82**, 2440–2442 (2003).
17. M. Dumont, Z. Sekkat, R. Loucif-Saibi, K. Nakatani, and J. A. Delaire, "Photoisomerization, photo-induced orientation and orientational relaxation of azo dyes in polymeric films," Nonlinear Opt. **5**, 395 (1993).

IOP PUBLISHING JOURNAL OF PHYSICS D: APPLIED PHYSICS

J. Phys. D: Appl. Phys. **41** (2008) 235502 (6pp) doi:10.1088/0022-3727/41/23/235502

Local photo-assisted poling of azo copolymer films by scanning probe microscopy

F S-S Chien[1], C Y Lin[2] and C C Hsu[2]

[1] Department of Physics, Tunghai University, Taichung, Taiwan
[2] Department of Physics, National Chung-Cheng University, Chiayi, Taiwan

E-mail: fsschien@thu.edu.tw

Received 19 June 2008, in final form 30 September 2008
Published 14 November 2008
Online at stacks.iop.org/JPhysD/41/235502

Abstract

Azo copolymers are nonlinear-optical materials, in which polar orientation can be induced by optical poling or electrical poling. We report a new efficient approach to performing photo-assisted poling (PAP) by atomic force microscopy (AFM) for azo copolymer films containing disperse-red-1 chromophores, and to characterize the polar orientation by electrostatic force microscopy (EFM) at the submicrometre scale. Both PAP and contact electrification effects can be generated by the physical interaction between the probes and the films. We demonstrated that these two effects can be distinguished by the relationship between the signs of the charges (bound charges and transferred charges) and the probe bias. Finally, we achieve local PAP far below the glass transition temperature by AFM operated in the tapping mode, and the response of the polar chromophores to local PAP can be studied by EFM.

(Some figures in this article are in colour only in the electronic version)

1. Introduction

The copolymer film containing disperse red 1 (DR1) is a photoreactive material that has been attracting much attention in the past few years, because DR1 is a polar, nonlinear-optical chromophore, exhibiting unique optical behaviours [1]. DR1, the push-pull derivative of azo-benzene molecules, has two isomers, *trans* and *cis* forms, which undergo the *trans* $\Leftrightarrow$ *cis* isomerization by optical pumping (referred to as photoisomerization). Molecular orientation anisotropy is built up optically in the copolymers after several cycles of *trans* $\Leftrightarrow$ *cis* photoisomerization pumped by a linearly polarized light. This is the so-called photo-induced orientation (PIO). In the opposite effect, an anisotropic DR1 copolymer can be disordered by light, called photo-induced disorientation (PID). Therefore PIO and PID offer the opportunity to manipulate the optical properties of photoreactive copolymer films. Many studies have demonstrated potential applications of DR1 copolymers for active waveguide components [2], frequency conversion [3], index grating [4] and image storage [5, 6].

There is considerable interest in moving the applications of photoreactive materials towards the nanometre scale. It is demonstrated that two-photon photopolymerization can make three-dimensional features on a resin for functional devices with a subdiffraction-limit spatial resolution of 120 nm [7]. Also, movement of azo polymers beyond the diffraction limit, induced by metal-tip-enhanced near-field illumination, was utilized to produce a protrusion with sub-50 nm full width at half maximum [8]. Recently, micrometre-scale polarization storage in the DR1-PMMA copolymer has been achieved. Various optical methods to write and read the polarization ($\vec{P}$) are demonstrated; writing by two-photon absorption (TPA) and reading by reflection laser confocal microscopy [9], or writing by the excitation of coherent fundamental (ω) and harmonic (2ω) lasers and reading by SHG [10], or writing by disorientation induced by TPA on a corona-poled anisotropic film and reading by second harmonic generation (SHG) measurement [11]. Both TPA and SHG are nonlinear-optical reactions, to which light is confined in the focal point to a volume of order λ^3 (λ: wavelength of incident light) to provide higher spatial resolution than conventional optical methods. However, the minimum poled or unpoled spots can be generated is about 2 μm in diameter and is still above the diffraction limit. In addition, there is an intrinsic problem

in SHG measurement of the polar orientation; the probe beam can cause a pronounced disturbance to the molecular orientation. Therefore, SHG measurement is not suitable in repeated reading and advanced studying of the dynamic response of the polar molecules to optical and electrical poling at subwavelength regions. Consequently, there is a stringent need for efficient approaches to both generate and characterize the local polar orientation well below the diffraction limit.

We employed scanning probe microscopy (SPM) to perform local photo-assisted poling (PAP) far below the glass transition temperature of DR1-PMMA copolymer thin films [12, 13]. The probe acts as both an electrode to apply an electric field ($\vec{E}$) by atomic force microscopy (AFM) and a sensor to detect $\vec{P}$ *in situ* by electrostatic force microscopy (EFM) [14–16]. However, two kinds of electric effects, poling and contact electrification (CE) [17], can be introduced by the interaction between metallic probes and insulating polymers, and both effects generate surface charges (bound charges σ_b and transferred charges σ_t) on the copolymers. Taking advantage of the difference between their natures, we demonstrate that these two effects can be distinguished by the relationship between the polarities of the charges generated and probe bias. Then PAP can be done without CE as the physical contact with the copolymer is handled cautiously. In this paper, we first verify that EFM is able to analyse the local variation of $\vec{P}$ on the film. EFM succeeded in mapping a two-dimensional depoled grid on a corona-poled film. Secondly, CE and PAP were separately performed and characterized by AFM and EFM, to show how they are distinguished by the sign of charges. Finally, we report that the kinetics of $\vec{P}$ produced by local PAP is a bi-exponential function of poling time.

2. Experiment

The DR1-PMMA copolymer was dissolved in chloroform and filtered with a 250 nm filter. Then it was spin-coated on a glass plate, which has an indium tin oxide (ITO) layer on the top surface as the bottom electrode for PAP. The films were subjected to a post-bake at 80 °C for 1 h. The DR1 chromophores in the spin-coated films are random oriented and centrosymmetric distributed. The thickness of the films is about 0.1–1 μm and the absorption peak is at 470 nm. In this study, poled and unpoled films were used for PID and PAP, respectively.

The poled film was prepared by corona poling. The film was kept at 120 °C (near its glass temperature, 125 °C) for 20 min, while an electric field of $-5\,\mathrm{kV\,cm^{-1}}$ was applied. Therefore $\vec{P}$ remains upward and the surface bound charge density $\sigma_b(=\vec{P}\cdot\hat{n})$ is positive, where $\hat{n}$ is the unit vector of surface normal. For PID, the poled sample was placed on a translation stage of the laser writing system with a travelling speed of $1.5\,\mathrm{mm\,s^{-1}}$. A focused and circularly polarized 514 nm argon laser with a power density of $2\,\mathrm{mW\,cm^{-2}}$ and a spot size of 6 μm was used to selectively depole the sample by PID.

A commercial SPM was utilized to scan the topography and conduct local PAP (by AFM) and characterize the polarization or surface charge (by EFM). A linearly polarized 473 nm, $710\,\mathrm{mW\,cm^{-2}}$ solid state laser with 3 mm diameter was used for local PAP. The illumination power was controlled by an attenuator. The EFM was operated in lift mode with a lift height of 30–50 nm to map the polarization of the DR1-PMMA thin films. The Si-based cantilever is metallic-coated with Ti–Pt double layers. The nominal radius of the probe apex is 20 nm. The nominal force constant and resonant frequency (f_0) of the cantilevers are 2–5 $\mathrm{N\,m^{-1}}$ and 65–70 kHz, respectively. The cantilever was stimulated at a fixed frequency near f_0. A sensing bias (−3 or +3 V) was applied to the probe during EFM mapping. The Coulomb force between the biased probe and σ_b, given by $-\sigma_b\vec{E}$, introduces an extra force gradient to the probe, leading to a shift of resonant frequency. The phase of the cantilever (ϕ) responds sensitively to the extra force gradient and the EFM maps the phase shift ($\Delta\phi$) of the cantilever with a lock-in amplifier to observe the variation of external force over the surface. An attractive/repulsive extra force causes a negative/positive phase shift, corresponding to a lower/higher (darker/brighter) EFM signal level. Therefore, given the imaging bias, the grey scale of the EFM images can represent both the magnitude and the sign of surface charges. The determination of the sign of the surface charges is critical to judge which effect (PAP or CE) induces the charges.

3. Results and discussion

3.1. Characterization of a PID-induced pattern by EFM

First, we demonstrate the capability of EFM to characterize the polarization of the copolymer films. A two-dimensional depoled grid of 20 μm pitch on a poled film was made by PID with direct laser writing. The grid was depoled, because the molecular orientations became isotropic due to the angular hole burning and angular redistribution after several *trans* ⇔ *cis* transition cycles, but the unwritten squares kept their polar orientation. Figure 1 shows the topographic AFM and electric EFM images. The surface relief can be observed in the topographic image (figure 1(*a*)). That is formed by the laser-induced molecular movement (i.e. mass transportation) at the film [18]. This grid relief about 1 nm high is a good reference for locating the grid during EFM imaging. The EFM images, figures 1(*b*) and (*c*), were taken with a sensing bias of −3 V and +3 V, respectively. Good coherence is shown between the topographic and the EFM images. However, the contrast of the EFM images reverses as the sign of the sensing bias changes. There are two components, Coulomb force and capacitive force, contributing to the EFM signal. The capacitive force varies with the surface relief and is always attractive regardless of the sign of the sensing bias, but the Coulomb force changes its direction with the sign of the sensing bias. The reversal of EFM contrast with sensing bias indicates that it is the Coulomb force between local charges and the biased probe, and the contribution of the minor surface relief can be ignored. From the relation of the signs of the bias and the contrast of EFM images, we assure that the charge is positive in the squares (marked by the dotted box), which agrees with our expectation to the corona-poled film, and proof that the variation of $\vec{P}$ in the DR1-PMMA films can be detected by EFM.

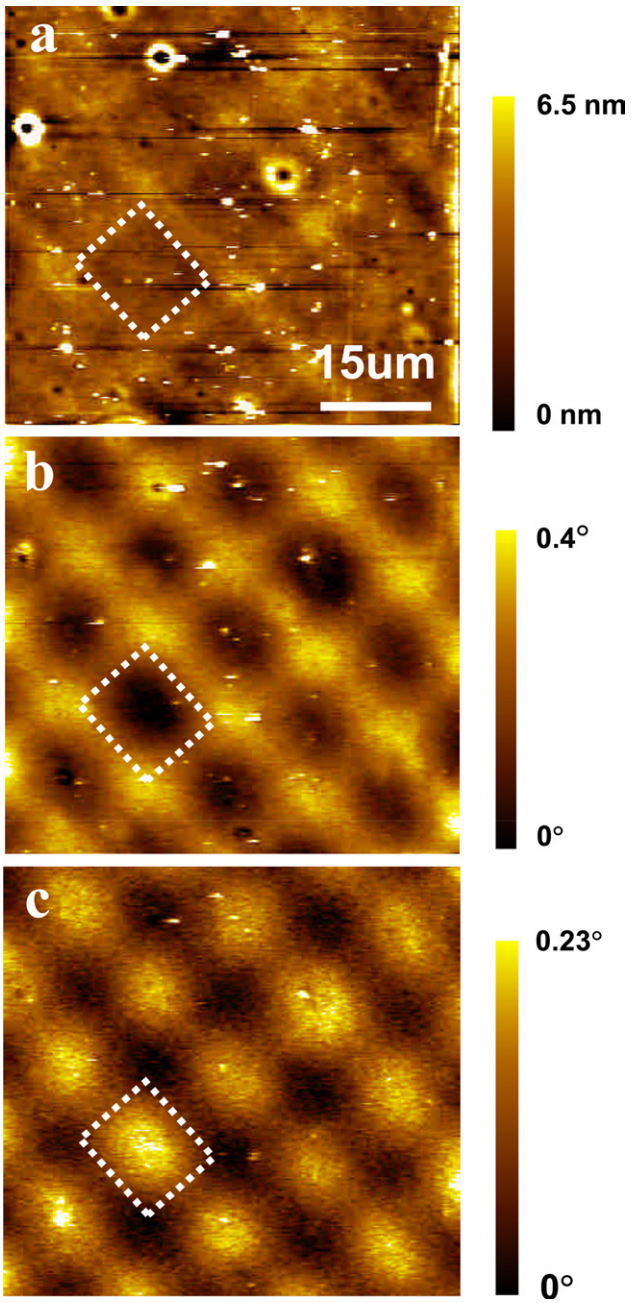

Figure 1. Topography taken by AFM (*a*) and polarization by EFM with −3 V and +3 V sensing bias (*b*) and (*c*) of the corona-poled DR1-PMMA copolymer film with a 2D depoled grid pattern generated by photo-induced disorientation. The squares marked by dotted lines are to indicate one of the corona-poled areas possessing positive bound charges.

3.2. CE by a biased probe

It is important to distinguish the effects of local PAP from CE by EFM. CE between metal and copolymer can be described by the charge injection between metals to copolymers. The distribution of the density of states of copolymers is presented by a double Gaussian, consisting of empty acceptor states and filled donor states (figure 2) [17]. For PMMA, the peaks of acceptor and donor states are at −2.0 eV and −6.1 eV, respectively. The centroid of the charge states ($\langle E \rangle = -4.1$ V) separates the Gaussians of acceptor and donor states, defined

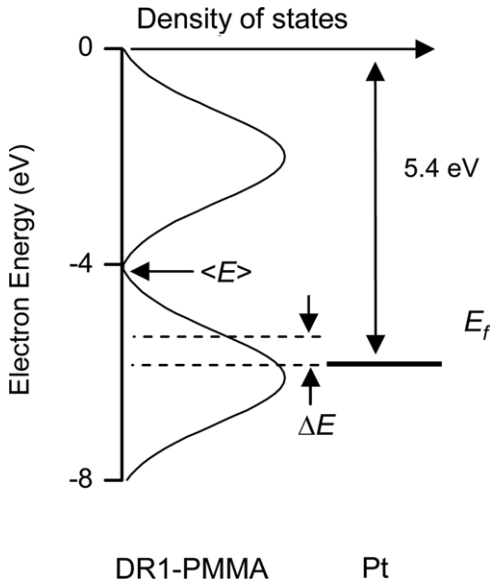

Figure 2. Spectrum of electron density of states of the DR1-PMMA, showing the double Gaussians with respect to the Fermi energy of Pt. The half width of the Gaussian is 0.845 eV. The DR1 molecules contribute a slight shift to the spectrum, which is ignored because it does not affect the interpretation of CE [17].

by the initial charge-neutral condition. The net density of exchange charges is expressed as

$$\sigma_t \propto \int_{E_F}^{E_F+\Delta E} \rho_D(E) f(E)\, dE - \int_{E_F-\Delta E}^{E_F} \rho_A(E)[1 - f(E)]\, dE, \quad (1)$$

where ρ_D and ρ_A are the density of donor and acceptor states, $f(E)$ is the probability that the state is occupied and $1 - f(E)$ is the probability that the state is unoccupied. E_F is the Fermi energy of Pt (5.4 eV) and ΔE, the transfer window of the metal, is approximately 0.4 V. The first term on the right of equation (1) represents the amount of charges injected from the donor states to the metal and the second term represents that from the metal to the acceptor states. If E_F aligns in energy with the donor (acceptor) states, CE is dominated by the injection from donor states to the metal (from the metal to acceptor states), and the transferred charges are positive (negative).

We verify the local CE effect by SPM on copolymers. AFM was operated in contact mode with a contact force of about 10 nN. The probe scanned over three strip areas (each of $0.5 \times 2.5\,\mu m^2$) at a speed of $1\,\mu m\,s^{-1}$, applied with writing biases (V_w) of 0 V, +3 V and −3 V, respectively. Figure 3 shows the topographic and the EFM images taken with a −3 V sensing bias. The negative EFM contrast of the first two strips (written with 0 and +3 V) indicates that an attractive force acts on the probe and positive charges are possessed there. This is because the Fermi level E_F of the Pt-coated probe aligns with donor states, while the probe was biased with 0 and +3 V. The positive contrast of the third strip (written with −3 V) indicates an opposite force and charges, for E_F aligns with acceptor states. Local charge transferring between probes and copolymer is governed by the CE model given in equation (1), and the sign of σ_t is determined by the relative position between the E_F level

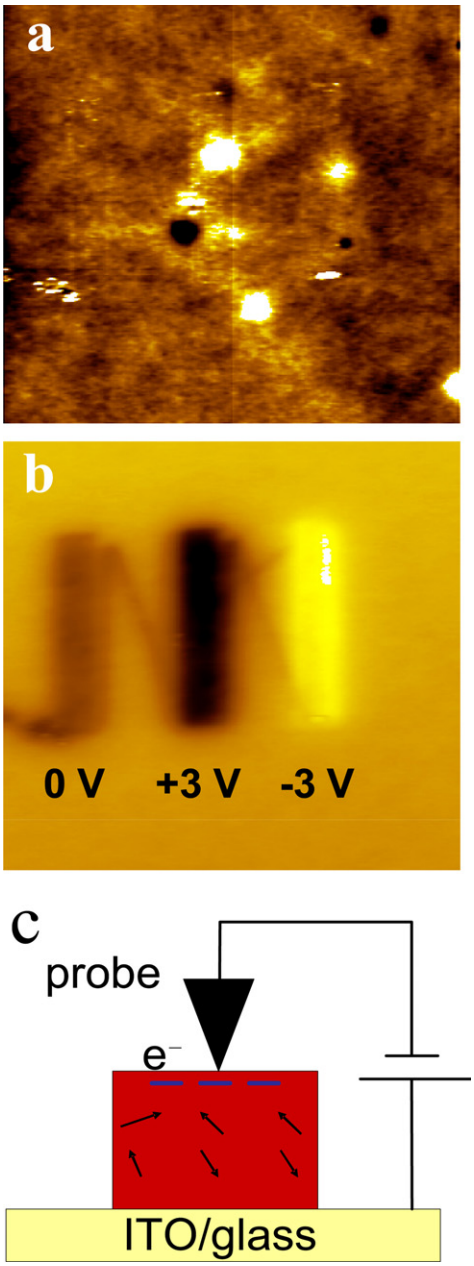

Figure 3. (*a*) $5 \times 5\,\mu m^2$ topographic image (grey scale = 2 nm), (*b*) EFM image illustrating the surface charges produced by CE with the writing bias of 0 V, +3 V and −3 V, respectively (grey scale = 9°) and (*c*) schematic of the relationship between the bias and transferred charges of the CE effect with a negative-biased probe.

of Pt and density of states of the copolymer. Typically, the sign is the same as that of V_w, as $|V_w|$ is greater than $|E_F - \langle E \rangle|$. Figure 3(*c*) illustrates the relationship between V_w and σ_t; a negative-biased probe induces negative σ_t due to the CE effect.

3.3. Local PAP by a biased probe

The polarization $\vec{P}$, generated by PAP, is parallel to $\vec{E}$, because the *cis*-chromophores are rotated by the torque $\vec{P} \times \vec{E}$, so the sign of σ_b is opposite to that of V_w. For instance, a negative-biased writing probe induces a positive bound charge σ_b at the surface (figure 4(*a*)), which is opposite to transferred charges

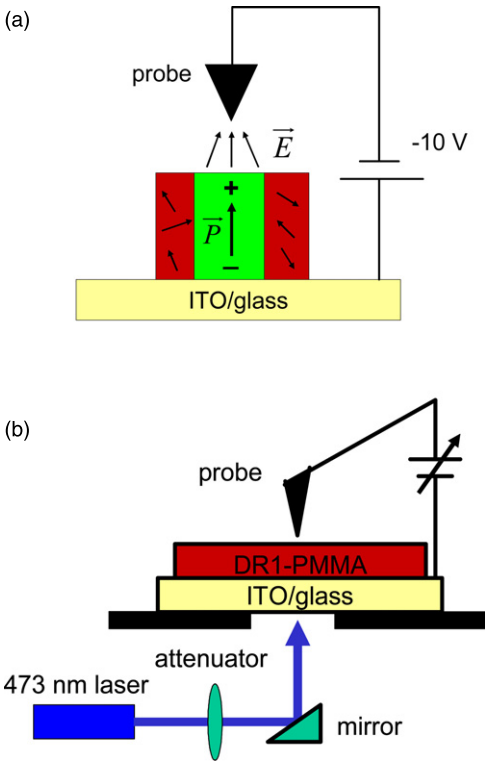

Figure 4. (*a*) Schematic of the relationship between the bias and polarization/bound charges associated with the local poling by a negatively biased probe and (*b*) the local PAP with an illumination of a laser source from the back side.

σ_t induced by the CE effect (figure 3(*c*)). Therefore, one can distinguish σ_b from σ_t by the relationship of charge signs and writing bias, due to the dissimilarity between the nature of PAP and the CE effects.

For implementation of local PAP by AFM, V_w was applied to the probe for poling and a linearly polarized diode-pumped solid state laser was used to stimulate the photoisomerization (figure 4(*b*)) [12]. An unpoled film (without corona poling) was subjected to local PAP. First we have to prove that CE can be avoided when the probe is biased. To do so, AFM was operated in tapping mode to reduce the friction force and the period of physical contact during poling. The oscillating amplitude of cantilevers is about 40 nm. Firstly, $V_w = +10$ V was applied without illumination, and no EFM signal was observed. That means when the probe is tapping, the CE is far less effective, which is under the detection limit of our EFM. The oscillating probe gently touches the film, so no detectable charge exchanges under the contact force (<10 nN), which is the same order as the contact force in contact mode. In other words, the magnitude of charge exchange described by equation (1) depends on both the magnitude of the force and the type of force (normal or frictional). The friction force in contact mode is significant to CE.

It is very surprising that probe poling failed without the assistance of photoisomerization. Even the local field is as high as $\sim 10^6\,V\,cm^{-1}$, but not strong enough to rotate the *trans*-chromophores. This indicates that the mobility of *trans*-chromophores is so low that the intense field is not able to move them.

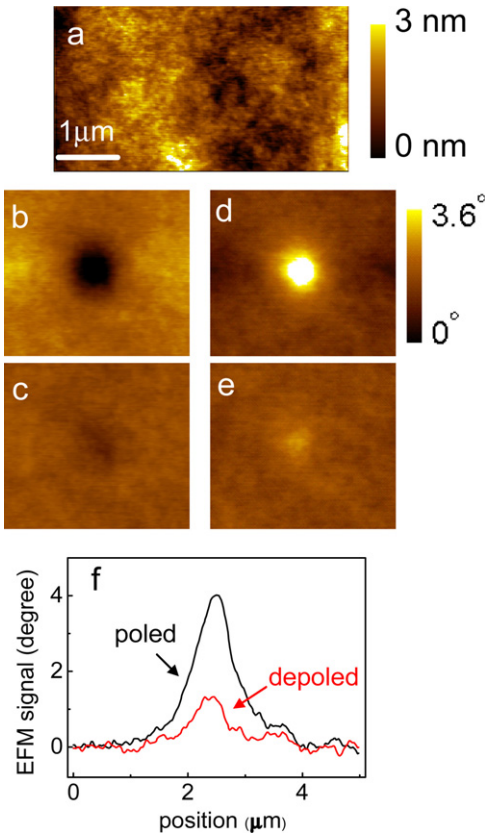

Figure 5. (*a*) $5 \times 3\,\mu m^2$ topographic image of the copolymer film, (*b*) and (*c*) EFM images of the spot poled by −10 V bias and depoled by photoisomerization, respectively, (*d*) and (*e*) EFM images of the spots poled by +10 V and depoled, respectively, and (*f*) the cross-sectional profile across the centres of (*d*) and (*e*). The size of the EFM images is $3 \times 3\,\mu m^2$.

Secondly, a 'poled' spot was produced by PAP under a writing bias of −10 V and illumination of the 1.5 mW cm^{-2} laser for 360 s. Figures 5(*a*) and (*b*) show the topographic and EFM images (with a −3 V sensing bias) taken simultaneously. There is no surface relief induced by the electric field. The negative contrast of EFM image at the spot indicates the force is attractive. This means that the corresponding charges are positive (opposite to the sign of V_w), and the charges should be bound charges σ_b, attributed to the polar anisotropy. Then, the spot can be depoled after the illumination with the same laser power for 60 s without a bias, as shown with the EFM image (figure 5(*c*)). The polarization is erased, due to PID. The σ_t do not respond to illumination, so it is evidence that the bound charges are generated. At the same location, we made another spot with an opposite writing bias, +10 V. The topography is similar to that shown in figure 5(*a*), and its EFM image has a positive contrast (figure 5(*d*)). Therefore, the charges are negative, consonant with our argument for σ_b again. The spot was depoled again after illumination without a bias (figure 5(*e*)). The cross-section profiles of figures 5(*d*) and (*e*) indicate there is little residual polar orientation after illumination. We attribute the residual polar orientation to the angular redistribution (see below) of the chromophores due to photoisomerization, where the polarization of the laser is horizontal.

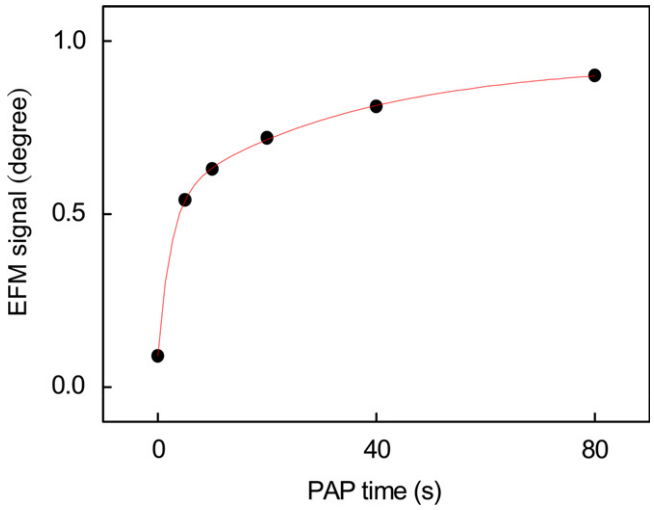

Figure 6. Kinetics of the polarization with the PAP time. The line is fitted with the bi-exponential function in equation (2).

Hence, it is evident that AFM can manipulate the orientation of DR1 chromophores through PAP. The DR1 chromophores are pumped to the *cis* form by *trans* → *cis* photoisomerization. For *cis*-chromophores have a higher mobility, angular diffusion occurs in the presence of the local field and the local polar orientation is built up. The diameter of the poled spot is only 500 nm, which is smaller than those poled/depoled spots (several micrometres) generated by all optical methods [9–11]. The spot size is controlled by the extents of the electric field and the laser field. The electric field is dominated since it is focused at the probe apex. The lateral distribution of the electric field is a Gaussian-like function. However, as the period of local PAP is about the order of characteristic time of angular redistribution (see below), the extent of the PAP effect (i.e. the spot size) should be about the extent of the electric field. We believe the spot size can be reduced, if the bias increases and the period of PAP decreases.

The response of chromophores to PAP at the submicrometre scale can be studied by EFM. We plot the magnitude of the EFM signal at the centre of the poled spot (under a −2 V writing bias and 0.7 mW cm^{-2} illumination as a function of the PAP time (t) (figure 6). Apparently, $P(t)$ can be well described by a bi-exponential function, increasing with t,

$$P(t) = P_0 - A_1 \exp(-t/\tau_1) - A_2 \exp(-t/\tau_2), \qquad (2)$$

where P_0 is the steady-state polarization, and $\tau_1 (= 2.4\,s)$ and $\tau_2 (= 34\,s)$ are the characteristic times of the chromophores to PAP, and A_1 and A_2 are coefficients of the exponential terms. Presumably, $P(t)$ is dominated by two processes with different characteristic times. We suggest these two processes are the fast *trans* → *cis* transition and slow molecular rotation, correlated with the angular hole burning and the angular redistribution, respectively, reported by Hsu *et al* [19]. Although the power density we applied for PAP is one order of magnitude smaller than that (12 mW cm^{-2}) for PID in [19], both τ_1 and τ_2 of PAP are shorter than those of PID (5.9 and 163.9 s). We attribute this to the electric field of PAP, which enhances the possibility to the molecules

pointing in the same direction. The polarization is stable, as the temperature far below the glass transition temperature of the copolymer. Typically, the polarization can retain over 10 h at room temperature. To understand the kinetics of polar chromophores under local PAP, further investigation with SPM is necessary.

4. Conclusions

We demonstrate the feasibility of achieving local PAP on a DR1-PMMA copolymer film by AFM and the polar anisotropy of DR1 chromophores is observed by EFM. This approach opens a new access to both producing polar anisotropy in the photoreactive polymer films, and to investigating the kinetics of the polar molecules reacting to PAP at the submicrometre scale, which is hardly achieved by other optical means. A 2D depoled grid on an anisotropic film is employed to verify the capability of EFM in analysis of the polarization on the film. Both PAP and CE effects are performed with SPM. The dissimilarity between these effects is addressed, and these effects can be distinguished by the relationship between the signs of the induced charges and the writing bias. The local PAP is achieved when the probe is operated in tapping mode and the induced polarization is erased by laser illumination. The polarization produced by local PAP increases as a bi-exponential function of the period of PAP.

Acknowledgments

The authors gratefully acknowledge the financial support from the National Science Council (NSC), Taiwan, under the Grant Nos NSC 96-2112-M-029-005-MY3 and NSC 95-2112-M194-014.

References

[1] Sekkat Z and Knoll W 2002 *Photoreactive Organic Thin Films* (San Diego, CA: Academic) and references therein
[2] Donval A, Toussaere E, Hierle R and Zyss J 2000 *J. Appl. Phys.* **87** 3258
[3] Martin G, Ducci S, Josse D and Zyss J 2003 *Appl. Phys. Lett.* **83** 1086
[4] Zhang W, Bian S, Kim S I and Kuzyk M G 2002 *Opt. Lett.* **27** 1105
[5] Sekkat Z, Wood J, Knoll W, Volksen W, Miller R D and Knoesen A 1997 *J. Opt. Soc. Am.* **14** 829
[6] Matsuoka N, Kitaoka K, Si J, Fujita K and Hirao K 2000 *Opt. Commun.* **185** 467
[7] Kawata S, Sun H B, Tanaka T and Takada K 2001 *Nature* **412** 697
[8] Ishitobi H, Tanabe M, Sekkat Z and Kawata S 2007 *Appl. Phys. Lett.* **91** 091911
[9] Maeda M, Ishitobi H, Sekkat Z and Kawata S 2004 *Appl. Phys. Lett.* **85** 351
[10] Bidault S, Gouya J, Brasselet S and Zyss J 2005 *Opt. Express* **13** 505
[11] Gindre D, Boeglin A, Fort A, Mager L and Dorkenoo K D 2006 *Opt. Express* **14** 9896
[12] Sekkat Z, Kang C-S, Aust E F, Wegner G and Knoll W 1995 *Chem. Mater.* **7** 142
[13] Blanchard P M and Mitchell G R 1993 *Appl. Phys. Lett.* **63** 2038
[14] Terris B D, Stern J E, Rugar D and Mamin H J 1989 *Phys. Rev. Lett.* **63** 2669
[15] Dianoux R, Martins F, Marchi F, Alandi C, Comin F and Chevrier J 2003 *Phys. Rev.* B **68** 045403
[16] Xu Q and Hsu J W P 1999 *J. Appl. Phys.* **85** 2465
[17] Fabish T J and Duke C B 1977 *J. Appl. Phys.* **48** 4256
[18] Barrett C J, Natansohn A L and Rochon P L 1996 *J. Phys. Chem.* **100** 8836
[19] Hsu C-C, Lin J-H, Huang T-H and Harada K 2003 *Appl. Phys. Lett.* **82** 2440

Fabrication of spatial modulated second order nonlinear structures and quasi-phase matched second harmonic generation in a poled azo-copolymer planar waveguide

Jian Hung Lin[a], Ngoc Diep Lai[a], Chau Han Chiu[a], Chi-Yuan Lin[a], Georg W. Rieger[b], Jeff F. Young[b], Forest Shih-Sen Chien[c], and Chia Chen Hsu[a]

[a)]*Department of Physics, National Chung Cheng University, Ming Hsiung, Chia Yi 621, Taiwan*
[b)]*Department of Physics and Astronomy, University of British Columbia, Vancouver, V6T 1Z1 Canada*
[c)]*Department of Physics, Tunghai University, Taichung 40704, Taiwan*
cchsu@phy.ccu.edu.tw

Abstract: This work demonstrates that arbitrary types of spatially modulated second-order susceptibility ($\chi^{(2)}$) structures such as 1D and 2D, periodic and quasi-periodic structures can be obtained by using the combination of corona poling and direct laser writing (DLW) techniques. The fabrication technique is based on the photodepoling of azo-dye molecules caused by one-photon or two-photon absorption during the DLW process. Polarization and second harmonic generation (SHG) images of the fabricated structures were measured by electrostatic force microscope and SHG mapping techniques, respectively. Furthermore, quasi-phase-matched (QPM) enhanced SHG from a 1D periodically poled azo-copolymer planar waveguide is demonstrated using an optical parametric oscillator laser by scanning wavelength from 1500 to 1600 nm. The resonant wavelength of the QPM enhanced SHG is peaked at 1537 nm with FWHM ≅ 2.5nm.

OCIS codes: (190.4710) Optical nonlinearities in organic materials; (230.4320) Nonlinear optical devices; (190.2620) Nonlinear optics second harmonic and wave mixing.

References and links

1. Z. Sekkat and W. Knoll, *Photoreactive Organic Thin Films* (Academic Press, USA, 2002).
2. P. Prasad and D. J. Williams, *Introduction to Nonlinear Optical Effects in Molecules and Polymers* (John Wiley & Sons, USA, 1991).
3. D. S. Chemla and J. Zyss, *Nonlinear Optical Properties of Organic Molecules and Crystals* (Academic Press, USA, 1987).
4. J. Zyss, *Molecular Nonlinear Optics Materials, Physics, and Devices* (Academic Press, USA, 1994).
5. J. A. Armstrong, N. Bloembergen, J. Ducuing, and P. S. Pershan, "Interactions between light waves in a nonlinear dielectric," Phys. Rev. **127**, 1918-1939 (1962).
6. G. Kanarian, R. A. Norwood, D. Haas, B. Feuer, and D. Karim, "Phase-matched second-harmonic generation in a polymer waveguides," Appl. Phys. Lett. **57**, 977-979 (1990).
7. Y. Shuto, T. Watanabe, S. Tomaru, I. Yokohama, M. Hikita, and M. Amano, "Quasi-phase-matched second-harmonic generation in diazo-dye-substituted polymer channel waveguides," IEEE J. Quantum Electron. **33**, 349-357 (1997).
8. M. Jager, G. I. Stegeman, W. Brinker, S. Yilmaz, S. Bauer, W. H. G. Horsthuis, and G. R. Mohlmann, "Comparison of quasi-phase-matching geometries for second-harmonic generation in poled polymer channel waveguides at 1.5 μm," Appl. Phys. Lett. **68**, 1183-1185 (1996).
9. S. Tomaru, T. Watanabe, M. Hikita, M. Amano, Y. Shuto, I. Yokohoma, T. Kaino, and M. Asobe, "Quasi-phase-mateched second harmonic generation in a polymer waveguide with a periodic poled structure," Appl. Phys. Lett. **68**, 1760-1762 (1996).
10. G. Martin, S. Ducci, R. Hierle, D. Josse, and J. Zyss, "Quasiphase matched second-harmonic generation from periodic optical randomization of poled polymer channel waveguides," Appl. Phys. Lett. **83**, 1086-1088 (2003).

11. J. J. Ju, J. Kim, J. Y. Do, M.-S. Kim, S. K. Park, S. Park, and M.-H. Lee, "Second-harmonic generation in periodically poled nonlinear polymer waveguides," Opt. Lett. **29**, 89-91 (2004).
12. G. L. J. A. Rikken, C. J. E. Seppen, S. Nijhuis, and E. W. Meijer, "Poled polymers for frequency doubling of diode lasers," Appl. Phys. Lett. **58**, 435-437 (1991).
13. O. Sugihara, Y. Che, N. Okamoto, H. Fujimura, C. Egami, and S. Umegaki, "High-resolution periodically poled structure in diazo-dye-substituted polymer film based on direct electron-beam writing technique," Appl. Phys. Lett. **73**, 3028-3030 (1998).
14. O. Sugihara, M. Nakanishi, Y. Che, C. Egami, Y. Kawata, and N. Okamoto, "Single-pulse ultraviolet laser recording of periodically poled structures in polymer thin films," Appl. Opt. **39**, 5632-5637 (2000).
15. X. Ni, M. Nakanishi, O. Sugihara, and N. Okamato, "Fabrication of $\chi^{(2)}$ grating in poled polymer waveguide based on direct laser beam writing," Opt. Rev. **5**, 9-11 (1998).
16. H. Ishitobi, Z. Sekkat, and S. Kawata, "Photo-orientation by multiphoton photonselection," J. Opt. Soc. Am. B **23**, 868-872 (2006).
17. H. Ishitobi, Z. Sekkat, and S. Kawata, "Ordering of azobenzens by two-photon isomerization," J. Chem. Phys. **125**, 164718-164718-4 (2006).
18. D. Gindre, A. Boeglin, A. Fort, L. Marger, and K. D. Dorkenoo, "Rewritable optical data storage in azobenzene copolymers," Opt. Express **14**, 9896-9901 (2006).
19. M. Maeda, H. Ishitobi, Z. Sekkat, and S. Kawata, "Polarization storage by nonlinear orientational hole burning in azo dye-containing polymer films," Appl. Phys. Lett. **85**, 351-353 (2004).
20. X. Li, J. W. M. Chon, R. A. Evans, and M. Gu, "Two photon energy transfer enhanced three-dimensional optical memory in quantum-dot and azo-dye doped polymers," Appl. Phys. Lett. **92**, 063309-063309-3 (2008).
21. Z. Sekkat, J. Wood, E. F. Aust, W. Knoll, W. Volksen, and R. D. Miller, "Light induced orientation in a high glass transition temperature polyimide with polar azo dyes in the side chain," J. Opt. Soc. Am. B **13**, 1713-1724 (1996)..
22. R. Loucif-Saibi, K. Nakatani, J. A. Delaire, M. Dumont, and Z. Sekkat, "Photoisomerization and second harmonic generation in disperse one-doped and functionalized poly(methyl methacrylate) films," Chem. Mater. **5**, 229-236 (1993).
23. V. M. Churikov and C. C. Hsu, "Optical control of third-harmonic generation in azo-doped polymethylmethacrylate thin films," Appl. Phys. Lett. **77**, 2095-2097 (2000).
24. S. Bian, L. Li, J. Kumar, D. Y. Kim, J. Williams, and S. K. Tripathy, "Single laser beam-induced surface deformation on azobenzene polymer films," Appl. Phys. Lett. **73**, 1817-1819 (1998).
25. M. J. Ventura, M. Straub, and M. Gu, "Void channel microstructures in resin solids as an efficient way to infrared photonic crystals," Appl. Phys. Lett. **82**, 1649 (2003).
26. M. M. Fejer, G. A. Magel, D. H. Jundt, and R. L. Byer, "Quasi-phase-matched second harmonic generation: Tuning and Tolerances," IEEE J. Quantum Electron. **28**, 2631-2654 (1992).
27. N. D. Lai, J. H. Lin, W. P. Liang, and C. C. Hsu, "Precisely introducing defects into periodic structures by using a double-step laser scanning technique," Appl. Opt. **45**, 5777-5782 (2006).
28. R. Dianoux, F. Martins, F. Marchi, C. Alandi, F. Comin, and J. Chevrier, "Detection of electrostatic forces with an atomic force microscope: Analytical and experimental dynamic force curves in the nonlinear regime," Phys. Rev. B **68**, 045403 (2003).
29. H. Ishitobi, M. Tanabe, Z. Sekkat, and S. Kawata, "The anisotropic nanomovement of azo-polymers," Opt. Express **15**, 652-659 (2007).
30. V. Berger, "Nonlinear photonic crystals," Phys. Rev. Lett. **81**, 4136-4139 (1998).
31. N.G. R. Broderick, G. W. Ross, H. L. Offerhaus, D. J. Richardson, and D. C. Hanna, "Hexagonal poled lithium niobate: a two dimensional nonlinear photonic crystal," Phys. Rev. Lett. **84**, 4345-4347 (2000).
32. S. Saltiel and Y. Kivshar, "Phase matching in nonlinear $\chi^{(2)}$ photonic crystals," Opt. Lett. **25**, 1204-1206 (2000).
33. R. Lifshitz, A. Arie, and A. Bahabad, "Photonic quasicrystals for nonlinear optical frequency conversion," Phys. Rev. Lett. **95**, 133901-133901-4 (2005).
34. R. J. Bratfalean, A. C. Peacock, N. G. R. Broderick, K. G.allon, and R. Lewen, "Harmonic generation in a two-dimensional nonlinear quasi-crystal," Opt. Lett. **30**, 424-426 (2005).
35. E. Kim, Y.-K. Choi, and M.-H. Lee, "Photoinduced refractive index change of a photochromic diarylethene polymer," Macromolecules, **32**, 4855-4860 (1999).
36. M. W. McCutcheon, G. W. Rieger, I. W. Cheung, J. F. Young, D. Dalacu, S. Frederick, P. J. Poole, G. C. Aers, and R. L. Williams, "Resonant scattering and second-harmonic spectroscopy of planar photonic crystal microcavities," Appl. Phys. Lett. **87**, 221110(1-3) (2005).

1. Introduction

Nonlinear optical (NLO) polymer materials have attracted considerable attention due to their large NLO responses and ease of processing for devices such as electro-optic modulators, and frequency converters [1-4]. In particular, quasi-phase-matched (QPM) second harmonic generation (SHG) in periodically poled materials can result in efficient frequency conversion [5]. Previous studies have shown NLO polymer materials offer many advantages for realizing

QPM SHG, for example: low cost, fast response, large nonlinearity, and flexible processing options [6-11]. Various techniques have been employed to fabricate periodically poled structures (i.e., second-order susceptibility ($\chi^{(2)}$) grating) in polymer thin films such as serial grafting [7,9], periodic poling [8], photodepoling with photolithographic masks [10], ultraviolet (UV) photobleaching [12], direct electron-beam (EB) irradiation [13], two-beam interference [14], and direct laser writing (DLW) [15].

In the DLW technique, the non-zero $\chi^{(2)}$ induced by uniformly corona-poling a polymer thin film is locally erased by locally irradiating the film with a laser beam to that randomizes the molecular orientation alignment. By scanning the focused laser across the polymer thin film, a spatially modulated $\chi^{(2)}$ structure can be obtained. Compared with other techniques, the DLW approach is easier and more flexible for controlling the structural design and period, because no mask or etching is required. Okamoto *et al*. used the DLW technique to fabricate $\chi^{(2)}$ grating structures in a poled polymer thin film based on an one-photon absorption induced depoling mechanism [15]. One-photon absorption-based depoling can be done with relatively low power lasers, but two-photon absorption-based depoling [16, 17] using pulsed lasers can provide higher lateral (2D) spatial resolution for a fixed laser wavelength, and it also allows 3D control over the depoling structure, if there is a limited depth of focus over which absorption occurs. Previous work on two-photon absorption-based DLW demonstrated it is feasible for optical data storage applications [18-20].

In this work we demonstrate that complex 2D $\chi^{(2)}$ patterned structures, with no measurable surface topography, and minor modulation of the linear refractive index ($\Delta n < 0.01$), can be easily fabricated by DLW techniques using both one-photon and two-photon absorption induced photodepoling in azo-copolymer thin films. Azo-copolymer thin films have photoisomerization effect, which can easily induce molecular orientation randomization at low exposure dosage. In this work, we show they are suitable for generating pure photo depoling effect by employing DLW technique. Furthermore, as an example of the possible device applications of this technique, the QPM SHG properties of a periodically poled azo-copolymer planar waveguide obtained by DLW technique are investigated. To our knowledge this is the first measurement of QPM enhanced SHG in a $\chi^{(2)}$ periodic structure obtained by the DLW technique.

This paper is organized as follows. Section 2 presents the DLW fabrication techniques used to produce a variety of periodic and quasi-periodic $\chi^{(2)}$ structures. Section 3 shows the spatial modulation of molecular-orientation in 1D and 2D structures characterized by SHG and electrostatic force microscopy (EFM) mapping techniques. Section 4 shows the measured QPM SHG signal obtained from a periodically poled azo-copolymer planar waveguide obtained by the one photon DLW technique. Conclusions are drawn in Section 5.

2. Fabrication of periodic and quasi-periodic nonlinear structures

The polymer thin films were formed from a DR1-PMMA copolymer with 15% molar azo-dye concentration. The copolymer was dissolved in chloroform, and spin coated on the backside of an indium-tin-oxide (ITO) glass substrate after the copolymer solution had been filtered with a 250 nm filter. The copolymer thin films were then baked for 12 hours at 70 ^{o}C in an oven before use. Figure 1(a) shows the absorption spectrum and molecular structure of the DR1-PMMA copolymer. The film thickness was about 2 μm and its absorption band ranged from 400 to 600 nm, with an absorption peak at 470 nm. A corona poling technique was used to align the NLO molecules at 4.5 kV and T ∽100^{o}C for 45 minutes. The distance between the needle electrode and the copolymer thin film was about 1cm. The uniform poling area is about 1 cm^2.

After corona poling, the DLW technique was first applied to fabricate $\chi^{(2)}$ periodic structures on poled copolymer thin films based on one-photon absorption induced photodepoling. Figure 1(b) shows the experimental setup. A CW Argon laser with wavelength at 514 nm was used as the light source. An objective lens (OL) with numerical aperture (NA)

= 0.4 mounted on a z-directional translation stage was used to focus the circularly polarized laser beam on the sample and the focusing spot size obtained was about 6 μm. The sample was mounted onto a 2D motor-controlled stage. The lateral travel range and the resolution of the motor stage are 2.5 cm and 1 μm, respectively. The motor stage and shutter were controlled by a computer. The exposure dosage can be controlled by changing laser power, exposure time or the scanning speed of the motor stage. The typical average power used in this work was about 0.3 mW. A similar DLW setup was also used to fabricate $\chi^{(2)}$ periodic and quasi-periodic structures based on two-photon absorption induced photodepoling effect. The modifications in the setup are as follows: a Ti: Sapphire laser with central wavelength at 830 nm, 100 fs pulse width, and 80 MHz repetition rate was used as the light source; a high NA (=0.85) OL was used to focus the incident laser beam and the focusing spot size obtained was about 1 μm; a 3D piezoelectric translation (PZT) stage with a resolution of 1 nm was used to translate the samples in 3D. The average power used in two-photon DLW experiment was about 35 mW.

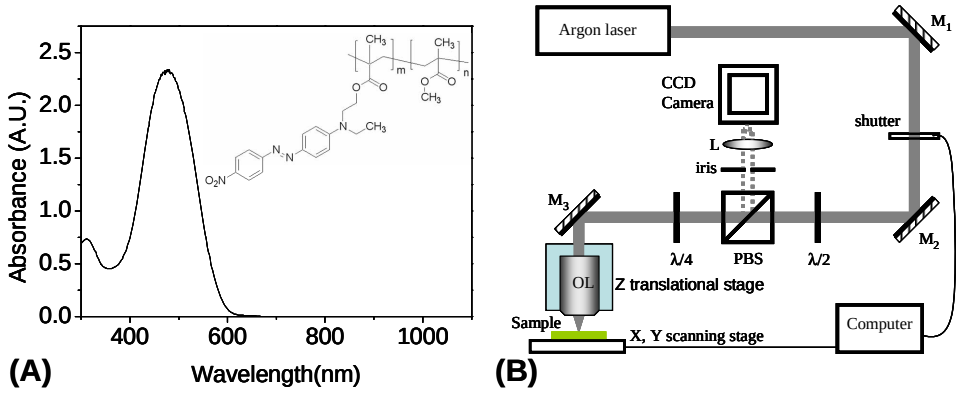

Fig. 1. (a) Absorption spectrum and molecular structure of the DR1-PMMA copolymer. (b) Direct laser writing setup for fabricating $\chi^{(2)}$ spatial modulated structures. L: lens; OL: objective lens; M_j (j=1,2,3): mirrors; λ/2: half-wave plate; λ/4: quarter-wave plate; PBS: polarized beam splitter.

During the DLW process, the second order nonlinearity of the corona-poled azo-copolymer thin film can be erased by the photodepoling effect [1, 10, 14-15, 21-22]. This photodepoling effect is initiated by the absorption of laser irradiation (by either one photon or two photon processes) in the azo-copolymer thin film, which leads azo-dye molecules to undergo many *trans* → *cis* → *trans* reversible photoisomerization cycles, and thus results in molecular orientation randomization at laser exposure sites [10, 21-22]. It is important to note that other photo-induced effects such as: bleaching [12, 23], mass transport [1, 24], and micro explosions [25] can also be generated during the DLW process, but these occur at much higher laser exposure dosages. These higher dosage effects result in significant linear-refractive index and surface morphology modulations that can induce large propagation loss and are unfavorable for most optical waveguide device applications [26]. Although a pure-photodepoling effect can also induce refractive index variation, it is shown below that the associated change of refractive index is much smaller than those induced at higher dosages.

3. Characterization of nonlinear $\chi^{(2)}$ structures

A SHG mapping technique was applied to map images of the $\chi^{(2)}$ structures. Its setup was the same as that of the two-photon absorption DLW technique except a photomultiplier tube covered with an interference filter (center wavelength = 415 nm) was added to detect the SHG

signal. The details of the laser scanning SHG mapping technique can be found in elsewhere [27]. The transverse resolution of this mapping technique was approximately 1 μm corresponding to the diffraction limit of the OL used (NA=0.85) at 830 nm. This laser scanning SHG mapping technique provides a direct measure of the $\chi^{(2)}$ spatial distribution in photo-depoled azo-copolymer samples. In Fig. 2(a) a high contrast 1D SHG modulation is clearly observed; and almost no SHG signal can be found from the exposure regions. In the one-photon absorption CW DLW experiment, we found when the laser writing average intensity and scan speed were chosen to be 0.01 mW/μm^2 and 2 mm/s, respectively, about 80% of the SHG response was removed at the laser exposed region in the corona poled azo copolymer thin film.

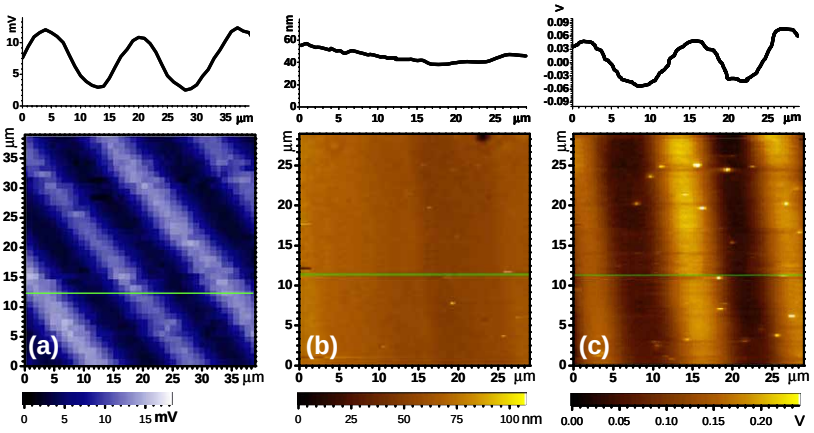

Fig. 2. (a) 40×40 μm^2 SHG image,and (b)-(c) 30×30 μm^2 AFM image and EFM image (with line profiles along the horizontal line at each top) of a 1D $\chi^{(2)}$ grating in a poled azo-copolymer thin film fabricated by DLW technique. The dashed lines in (a) and (c) indicate the line centers of the poled regions

The contrast of the electric polarization ($\vec{P}$) between the poled and depoled regions can be a significant evidence for the $\chi^{(2)}$ modulation. Therefore, a scanning probe microscope (SPM) was employed to measure the topography and electric polarization modulation based on atomic force microscope (AFM) and electrostatic force microscope (EFM) schemes [28] respectively. During EFM imaging, a metallic-coated probe, oscillating at the resonant frequency and biased by -8 V, was scanned across the sample surface at a fixed height to sense the force between the probe and the film. The surface bound charges with the charge density σ_b ($=\vec{P}\cdot\hat{n}$, where $\hat{n}$ is the surface normal unit vector) exert a Coulomb force ($-\sigma_b\vec{E}$) to the biased probe and results in a phase shift of the oscillating probe. By mapping the phase shift at different positions, the electric polarization distribution of the sample can be obtained. An additional attractive/repulsive force causes a minus/plus phase shift, corresponding to a lower/higher (darker/brighter) EFM signal level, so EFM is sensitive to both the amplitude and direction of $\vec{P}$, while the SHG measurement can determine the former only. Consequently, the EFM measurement result is also included in this work.

Figures 2(b) and 2(c) show the AFM and EFM images of the same 1D $\chi^{(2)}$ grating imaged in Fig. 2(a). The AFM image in Fig. 2(b) reveals that the sample after patterning with a 1D $\chi^{(2)}$ grating still possessed a very smooth surface; there are no signs of a periodic modulation of the sample texture. The result is different to a previous observation obtained by the same experimental irradiation scheme, in which a nanoscale surface deformation induced by a tightly focused laser beam was found [29]. The difference is due to our exposure dosage is below the threshold of inducing surface deformation. On the other hand, Fig. 2(c) clearly shows that the EFM image has 1D periodic modulation on electric polarization. In the bright

regions exposed to laser, the NLO molecules are randomly oriented so that the electric polarizations in those regions are zero or rather small. On the other hand, in the dark regions not exposed to laser, the force is attractive, indicating most NLO molecules are still aligned in the upward direction, which cannot be determined from the SHG image. In addition, EFM is a more favorable approach to investigate the polarization in NLO copolymers than SHG mapping, because EFM is based on the electric interaction between probe and polymer film, hardly disturb the molecular orientation from our experiences. Note that when the sample was exposed by high dosage of laser, mass transport and micro explosion of polymer material were induced and large modulations of surface topographic (> 100 nm) and refractive index ($\Delta n > 0.01$) were observed.

The variation of refractive index between poling and depoling regions also possibly contribute the contrast of EFM image. However, the modulation of refractive index is very shallow ($\Delta n < 0.01$), compared with its background index, so it is difficult to detect by EFM. In addition, the contrast of EFM image associated with the variation of refractive index is independent with the polarity of the imaging bias, but that associated with polarization modulation is reverse as the polarity of the bias changes. We observed such a reverse of contrast when we changed the polarity of the bias (because the sign of the force changed accordingly). Therefore, we assure the contrast of EFM is due to the variation of electric polarization, instead of the modulation of refractive index, inferring 1D $\chi^{(2)}$ modulation generated by DLW.

The $\chi^{(2)}$ response can be erased not only by one-photon absorption induced photodepoling effect but also by two-photon absorption induced photodepoling. Fig. 3(a) and (b) demonstrate SHG mapping images of a 2D hexagonal $\chi^{(2)}$ structure and a 2D circular $\chi^{(2)}$ structure fabricated using the two-photon DLW technique, respectively. The lattice constant in the 2D hexagonal $\chi^{(2)}$ structure and the radial distance between circles in the 2D circular $\chi^{(2)}$ structure are 4 μm. As illustrated in these two SHG mapping images, a high contrast ratio of 2D SHG spatial modulation and a near-zero SHG response at the laser exposure regions can be clearly observed in both structures. From additional optical microcopy and AFM measurements, we confirmed again that refractive index variation and surface modulation are small in both of these structures. For this two-photon absorption DLW experiment, pure photodepoling effect occurred when exposing copolymer thin films with 11.15 mW/μm^2 average intensity of the femtosecond laser pulse train for 50 ms, which corresponds to the exposure dosage about 490 mJ/cm^2. Under this exposure condition, more than 90% of the SHG response was erased in the exposed regions. To make sure the samples only experienced a pure photodepoling effect, we have reapplied corona poling to the previously exposed samples and performed an SHG mapping experiment again; we found the samples could generate a uniform SHG response just like that of obtained from a sample without exposing by laser irradiation.

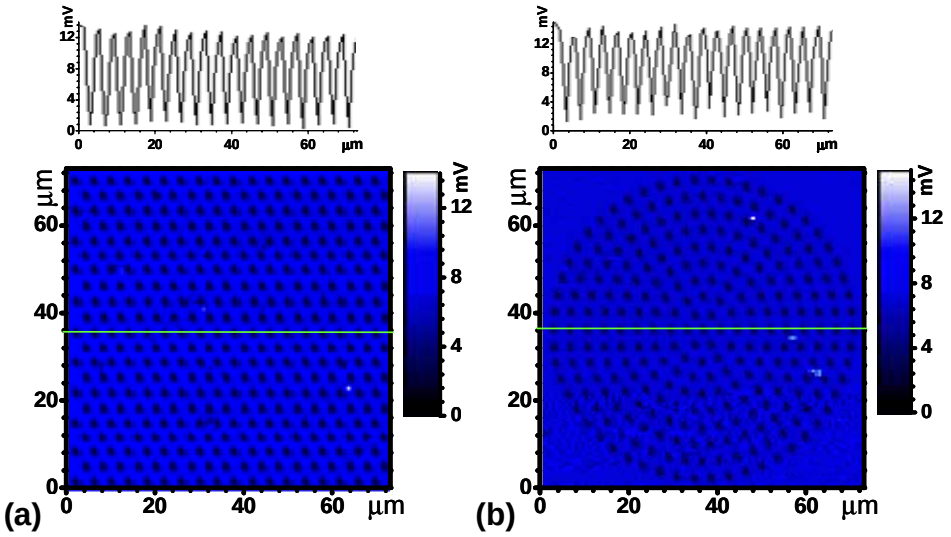

Fig. 3. The SHG mapping images in poled azo-copolymer thin films measured by the SHG mapping technique. (a) 2D hexagonal $\chi^{(2)}$ structure and (b) 2D circular $\chi^{(2)}$ structure with period = 4 μm, both fabricated by two-photon absorption DLW technique.

By scanning the focused femtosecond pulses beneath the surface of the sample, the two-photon absorption DLW technique can result in photodepoling throughout a thick film, whereas in the one-photon absorption DLW technique, strong absorption limits the penetration depth of the depoling irradiation [10]. Together with the above results, this suggests that the two-photon absorption DLW technique can be used to fabricate 3D polymer $\chi^{(2)}$ photonic crystals and photonic quasi-crystals. Those kinds of structures provide the possibility of multi phase matching and multi color parametric conversion and are potentially useful for spatial and temporal shaping of input beams through appropriately designed structures, [30-34].

4. Quasi-phase-matched SHG measurement

After characterizing the $\chi^{(2)}$ responses of structures obtained by the DLW technique, in this section QPM SHG of a 1D periodically poled azo-copolymer planar waveguide obtained by the one-photon absorption DLW technique is presented. To design an appropriate QPM SHG sample, the bulk TM mode refractive indices of a corona poled azo-copolymer thin film at four different wavelengths was measured using a prism coupler technique. The measured refractive indices at 632.8 nm, 845 nm, 1300 nm, and 1550 nm were fitted to a Sellmeier equation [35]

$$n^2(\lambda) = A + (B \times \frac{\lambda^2}{\lambda^2 - C}), \tag{1}$$

where n(λ) is the refractive index at the wavelength λ, and A, B and C are the fitting constants. The fitting result is shown in Fig. 4(a). The period for 1D QPM $\chi^{(2)}$ grating for collinear TM-in TM-out SHG conversion can be determined from [26]

$$\Lambda_q = q\Lambda = \frac{q\lambda_F}{2(n_{2\omega} - n_{\omega})} \tag{2}$$

where Λ is the grating period; q is the QPM order; λ_F is the fundamental wavelength; n_ω and $n_{2\omega}$ are refractive indices at fundamental and second harmonic wavelengths, respectively.

The period of a +/0 1D $\chi^{(2)}$ grating (q = 1) for different fundamental wavelengths were determined from Eqs. (1) and (2), and the result is shown in Fig. 4(b). Accordingly, a period of 12 μm was chosen for the $\chi^{(2)}$ grating period to observe QPM for a fundamental wavelength near 1510 nm.

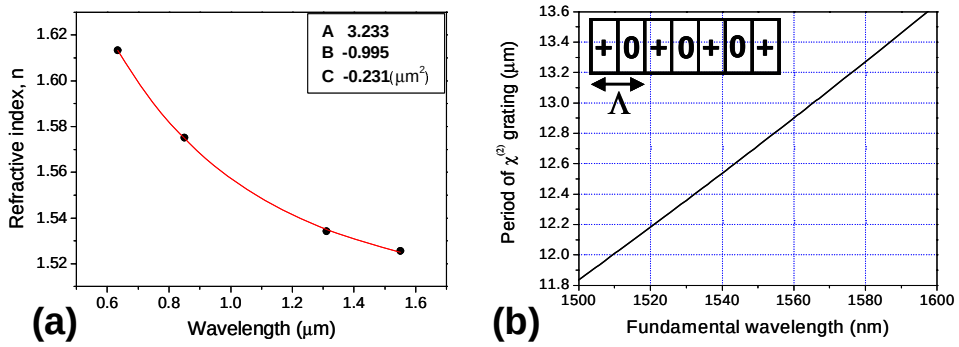

Fig. 4. (a) The TM mode (p-polarized) bulk refractive index of a corona poled azo-copolymer thin film as a function of wavelength. The dots are the experimental data measured by prism coupler technique and the red-solid line is the fit to the Sellmeier equation. A, B, and C in the inset are the fitting parameters. (b) The calculated QPM period value as a function of the fundamental wavelength for a 1D +/0 $\chi^{(2)}$ grating, assuming a TM-in TM-out geometry, and ignoring waveguide dispersion effects

A 1D $\chi^{(2)}$ grating with pitch 12 μm and an area of 10 mm × 2 mm was thus formed using one-photon DLW. The surface morphology, electric polarization and SHG mapping images of the 1D $\chi^{(2)}$ grating are the same as those shown in Fig. 2. Fig. 5(a) shows the experimental set up for measuring QPM SHG from the 1D periodic poled azo-copolymer planar waveguide. The signal output from an optical parametric oscillator (OPO), with wavelength tuning range from 1.3 to 1.6 μm, 100 fs pulse width, and 80 MHz repetition rate, was used as the fundamental beam [36]. The fundamental beam with average power of 20 mW was focused into the polymer planar waveguide (butt-coupling geometry) by a lens with focus length 1 cm and the SHG output was collected by a lens (f = 3 cm). The SHG output was analyzed using a grating spectrometer. It was found that both TE mode and TM mode fundamental beams were able to generate TM polarized QPM SHG. The $TM^{\omega} \rightarrow TM^{2\omega}$ conversion is related to $\chi^{(2)}_{zzz}$ (z is the electric filed poling direction) and the $TE^{\omega} \rightarrow TM^{2\omega}$ conversion is related to $\chi^{(2)}_{zxx}$. Since $\chi^{(2)}_{zzz}$ is much larger than $\chi^{(2)}_{zxx}$ for an electric poled thin film, the TM mode fundamental generated much stronger SHG compared to TE mode fundamental [2]. Consequently, only the TM mode fundamental results are presented here.

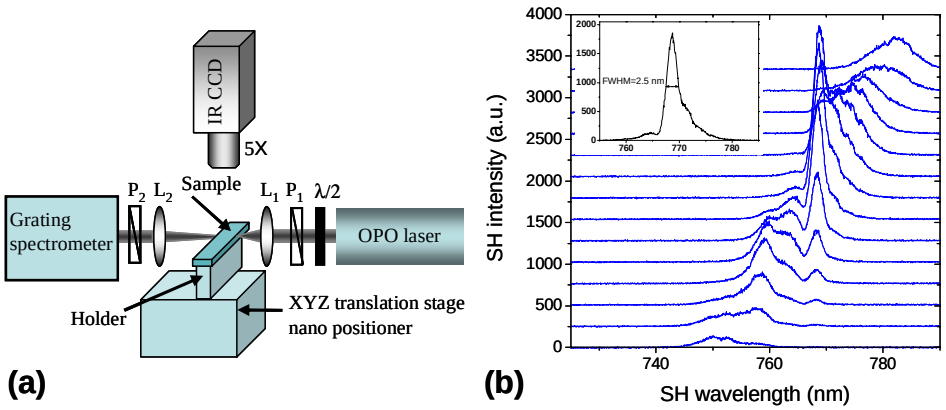

Fig. 5. (a) Experimental set up for measuring QPM SHG output spectra from a 1D periodic poled azo-copolymer planar waveguide. L1: focusing lens (f = 1cm); L2: collecting lens (f = 3cm); P_1 and P_2: polarizer; λ/2: half-wave plate. (b) SHG output spectra obtained by scanning fundamental wavelength from 1500 nm to 1565nm. Inset: close-up of the QPM SHG resonance mode peak at 768.5 nm. The FWHM of the resonant mode is 2.5 nm.

Figure 5(b) shows the normal incidence SHG output spectra of the 1D periodically poled azo-copolymer planar waveguide obtained by scanning the fundamental wavelength from 1500 nm to 1565 nm. The SHG spectra exhibit two QPM enhanced SHG peaks located at 768.5 nm (fundamental wavelength at 1537 nm) and 759 nm (fundamental wavelength 1518 nm). The former corresponds to converting fundamental waveguide mode TM_0^{ω} to second harmonic waveguide mode $TM_0^{2\omega}$ and the latter corresponds to the conversion from TM_0^{ω} to $TM_1^{2\omega}$. The fundamental wavelengths of these two QPM SHG resonant modes are close to our theoretically predicted value (1510 nm) shown in Fig. 4(b). When the fundamental wavelength is out of the resonance regions, for example at 1500nm, the SHG spectra are much weaker (about 20 times less than resonance case) and wider due to the existence of non-compensated phase mismatch between fundamental and second harmonic waves. The inset in Fig. 5 (b) shows a close-up of the QPM SHG resonance mode peak at 768.5 nm. The FWHM of the QMP SHG resonance mode is 2.5 nm.

5. Conclusions

A simple and efficient way to fabricate $\chi^{(2)}$ spatial modulated structures in azo-copolymer thin films is demonstrated. Various types of $\chi^{(2)}$ structures, including 1D gratings and 2D periodic and quasi-periodic patterns were fabricated by the combination of corona poling and either one-photon or two-photon absorption DLW. SHG, AFM and EFM mapping techniques were employed to show that SHG modulation depths as large as 90% could be obtained with no measurable surface topography and minor modulation of the linear refractive index ($\Delta n < 0.01$). This low power DLW technique, applied to DR1-PMMA, thus offers a flexible means of realizing "pure $\chi^{(2)}$" texture with feature sizes on the order of microns. This kind of structure has smaller propagation loss and it is more favorable for QPM SHG than those structures obtained by photobleaching, mass transport, and micro explosion.

To demonstrate a potential device application, QPM enhanced SHG from a 1D periodically poled azo-copolymer planar waveguide was measured. A QPM SHG resonant mode was identified at 1537 nm with 2.5 nm FWHM and with more than 20 times enhancement for TM_0^{ω} to $TM_0^{2\omega}$ conversion. Since the DLW technique is versatile for fabricating arbitrary $\chi^{(2)}$ patterned structures such as periodic and quasi-periodic, 1D, 2D and even 3D (by the two photon absorption DLW technique), it should be further explored for the fabrication of polymer based EO devices.

Acknowledgments

The authors gratefully acknowledge financial support from the National Science Council (NSC), Taiwan, under grant Nos. NSC 95-2120-M194-006 and NSC 95-2112-M194-014. N. D. Lai acknowledges the support of postdoctoral fellowship from NSC Taiwan. The support of the Natural Science and Engineering Research Council of Canada, and the Canadian Institute for Advanced Research is also gratefully acknowledged.